Chem Soc Rev

Engineered Nanomembranes for Smart Energy Storage Devices

Journal:	*Chemical Society Reviews*
Manuscript ID	CS-SYN-09-2015-000708.R2
Article Type:	Review Article
Date Submitted by the Author:	26-Nov-2015
Complete List of Authors:	Yan, Chenglin; Soochow University, School of Energy Wang, Xianfu; Soochow University, Chen, Yu; Soochow University, Schmidt, Oliver; IFW Dresden,

Engineered Nanomembranes for Smart Energy Storage Devices

Xianfu Wang, Yu Chen, Oliver G. Schmidt, and Chenglin Yan

Table of Content image and text

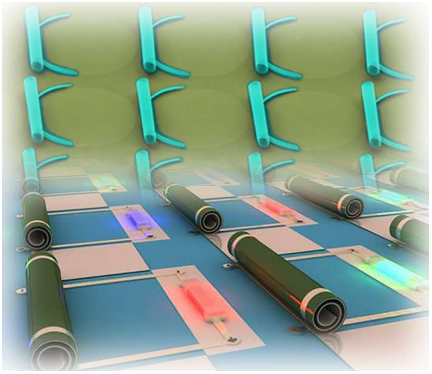

This review presents recent progress on engineered tubular and planar nanomembranes for smart energy storage applications, especially for fundamental electrochemical kinetics investigation.

Journal Name

ARTICLE

Engineered Nanomembranes for Smart Energy Storage Devices

Xianfu Wang,[a] Yu Chen,[a] Oliver G. Schmidt,[b,c] and Chenglin Yan[a]

Received 00th January 20xx,
Accepted 00th January 20xx

DOI: 10.1039/x0xx00000x

www.rsc.org/

Engineered nanomembranes are of great interest not only in large-scale energy storage devices, but also in on-chip energy storage integrated microdevices (such as microbatteries, microsupercapacitors, on-chip capacitors, etc.) because of the large active surface for electrochemical reactions, shortened paths for fast ion diffusion, and easy engineering for microdevice applications. In addition, engineered nanomembranes provide a lab-on-chip electrochemical device platform for probing the correlation between the electrode structure, electrical/ionic conductivity and the electrochemical kinetics as well as the device performance. This review focuses on the recent progress on engineered nanomembranes including tubular nanomembranes and planar nanomembranes, with the aim to provide a systematic summary of the fabrication, modification, as well as energy storage applications in lithium-ion batteries, lithium-oxygen batteries, on-chip electrostatic capacitors and micro-supercapacitors. A comprehensive understanding of the relationship between engineered nanomembranes and electrochemical properties of lithium ion storage with engineered single tube microbatteries, and micro-supercapacitors combined with their flexibility and transparency is discussed. Remarks on challenges and perspectives of engineered nanomembranes for further development in energy storage applications conclude this review.

1. Introduction

Being troubled by the gradual depletion of non-renewable resources like oil, coal, natural gas etc. and increasing environmental problems, such as pollution and global warming, new energy sources including hydro-electric power, wind, solar, tidal and geothermal power that are sustainable, safe and environmental friendly are urgently demanded. However, these dynamic resources vary with time and geographic conditions, which makes them cumbersome to be used stably and deterministically. For this reason, energy storage becomes a key component in the utilization of electricity generated from these intermittent renewable sources. [1-4] Among which, electrochemical energy storage devices such as rechargeable lithium ion batteries (LIBs) and supercapacitors (SCs) have attracted worldwide attention because of their vital roles as the dominant power sources for a range of applications, from portable electronics to electric vehicles (EVs), hybrid electric vehicles (HEVs), and even huge energy-storage systems. [5-14]

Among numerous nanostructures that have been fabricated for energy storage, two-dimensional (2D) nanomembranes have some superior properties including small weight, large exposed surfaces and specific facets, which interestingly, fulfill exactly the requirements for lithium storage. [15-19] Besides, 2D-like nanostructured materials – nanomembranes – are ideal materials for fast lithium storage, which require stability, high active surface area and open shortened path for lithium insertion/deinsertion. [16] In addition, the nanomembranes exhibit high mechanical stability, high flexibility, and good machinability, which are the right ingredients for fabricating micro-SCs and flexible SCs that may display huge potential in miniature, flexible, and wearable electronics. [20-24] In the past few years, two basic kinds of nanomembranes have been studied as high-performance electrodes for energy storage devices. One is the conventional 2D plane nanomembranes. The other is 3D tubular nanomembranes, which can be fabricated from the plane nanomembranes. Due to their unique structures and super properties, both the plane nanomembranes and tubular nanomembranes have been designed and explored extensively for high performance energy storage devices, especially LIBs and SCs. In particular, the single rolled-up tube batteries reviewed here are promising for fundamental research of voltammetry and electrochemical processes and can also be used as local on-chip energy supply or for driving ultra-compact autonomous microsystems.

Rolled-up nanotechnology is an advanced strategy to deterministically rearrange the geometry of nanomembranes by strain release. It can be a versatile method to roll nanomembranes of different functional materials and form a tubular structure by relaxing the intrinsic strain, thus allowing for enhanced tolerance towards stress cracking. The deposited inorganic nanomembranes coated on e.g. a polymer sacrificial layer can be released by dissolving the sacrificial layer with acetone, thus in this way be engineered into micro-

[a] School of Energy, College of Physics, Optoelectronics and Energy & Collaborative Innovation Center of Suzhou Nano Science and Technology, Soochow University, Suzhou 215006, China.
E-mail: c.yan@suda.edu.cn
[b] Institute for Integrative Nanosciences, IFW-Dresden, Helmholtzstrasse 20, 01069, Dresden, Germany.
[c] Merge Technologies for Multifunctional Lightweight Structures, Chemnitz University of Technology, Chemnitz 09107, Germany

/nanotubular structures (Fig.1a). Fig. 1b-i show examples of tubular structures rolled up from nanomembranes using this technology. Importantly, it is very convenient to place the tubular structure accurately on a chip, as preliminarily demonstrated in Fig. 1j for a SiO/SiO_2 tubular nanomembrane array.[25] So far, this technology has proven to be an intriguing approach for improving the electrochemical performance of various electrode materials. Moreover, rolled-up nanotechnology provides a facile way to fabricate microbatteries, which could scale down the size of batteries for the miniaturization of electronic devices and for on-chip energy supply for driving ultra-compact autonomous microsystems, thus paving the way for integration of microbatteries with other microdevices such as field effect transistors, photodetectors, memories, logic gates for on- and off-chip applications (Fig. 1k). It can also provide a platform for the fundamental research of voltammetry and electrochemical processes.

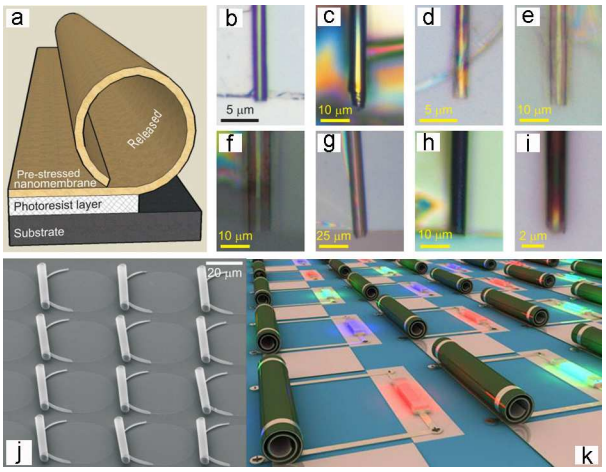

Fig. 1 (a) Schematic diagram of rolling-up a nanomembrane into a tube. Optical images of rolled-up nanomembranes (b) Pt, (c) Pd/Fe/Pd, (d) TiO_2, (e) ZnO, (f) Al_2O_3, (g) Si_xN_y, (h) Si_xN_y/Ag, and (i) diamond-like carbon. (j) SEM image of an array rolled-up SiO/SiO_2 nanomembranes. Reprinted with permission from ref. 28. Copyright 2008 Wiley-VCH Verlag GmbH & Co. KGaA, Weinheim (k) Concept diagram of on-chip integrated devices based on microbatteries.

This article reviews the recent development of engineered nanomembranes, including 3D tubular and 2D plane nanomembranes with focus on their applications in energy storage devices, such as LIBs, Li-O_2 batteries, capacitors, and SCs. A lab-on-chip electrochemical device platform based on microbatteries for probing the correlation between the nanomembrane electrode structure, electrical/ionic conductivity and the fundamental electrochemical kinetics is introduced. In the first part, we give a general introduction regarding the metrics of nanomembranes for energy storage devices. The second part starts with a brief introduction of rolled-up nanotechnology for nanomembrane engineering, followed with detailed description on their applications in LIBs, Li-O_2 batteries, single tubular batteries and capacitors and the analysis on nanomembrane structures and their energy storage performances. Fundamental research of voltammetry and electrochemical kinematics for lithium ion storage and different proton diffusion behavior are also highlighted. In the following section, a simple overview of the recent progress regarding LIBs based on 2D plane nanomembranes is given, and micro-SCs on graphene and composite planar nanomembranes are also introduced in detail with focus on their high energy and power densities, combined with a discussion of their flexibility, transparency, future challenges and opportunities for the fabrication of state-of-the-art micro-SCs. Finally, we briefly give some general remarks on several important aspects and challenges that are present in the current study and provide an outlook towards further development in engineered nanomembranes for energy-storage devices.

2. Tubular nanomembranes

In general, the Li^+ storage mechanisms for anodes can be classified into three types: [26] insertion reaction, alloying-dealloying, and conversion reaction. It is known that, for each reaction, one of the big challenges for Li^+ storage is electrode pulverization and consequent deterioration in cycling performance caused by the large volume changes and strain accommodation generated during lithiation/delithiation processes. On the other hand, electrode pulverization generated by stresses during Li^+ insertion/extraction also creates new interfaces, which will consume lithium and increase diffusion lengths, thus leading to performance degradation.[27] Therefore, if the strain caused by lithiation or delithiation can be released by electrode material composition and morphology, batteries with high capacity, long cycle life and high rate capability could be realized.

To this end, we introduced rolled-up nanotechnology as a new strategy to fabricate strain-released hierarchy micro-/nanostructures. The most attractive feature of these materials is “strain release”, during which the strain energy relaxes to a minimal level by rolling, so as to improve the capability to accommodate strain (stress) induced by Li^+ insertion/extraction, therefore enhancing the tolerance to stress cracking and preventing the electrode from pulverization. By using rolled-up nanotechnology, we have explored various tubular nanomembranes and studied their potential applications for enhancing Li^+ storage performance. In this part, beginning with the introduction of rolled-up nanotechnology, we focus on the evolution of tubular nanomembranes for Li^+ storage from silicon-based, germanium-based to composite tubular nanomembranes, and further discussion is included to highlight the intrinsic merits of tubular nanomembranes for Li^+ storage.

2.1 Rolled-up nanotechnology for nanomembrane engineering

Rolled-up nanotechnology is an approach to automatically rearrange 2D thin films into tubular geometry by releasing the strain in thin membranes.[28] So far, this technique has proven to be an intriguing approach for various promising applications, e.g. microelectronics,[29] biology,[30] optics[31] and energy storage[32]. It is worth noticing that rolled-up nanostructures possess

relaxed elastic strain energy, and as a result it opens up an excellent possibility for Li^+ storage due to the released strain introduced during the lithiation and delithiation processes.

Specifically, the residual strain present in thin membranes results in the change of film dimensions via either bending or wrinkling processes. The self-rolling process is mainly driven by the residual strain (stress) in nanomembranes, and the mechanism has been investigated in detail to quantitatively determine the wrinkling or bending/rolling. Figure 2 provides a simple model to illustrate the physical mechanism based on strain-stress theory. For simplicity, a bilayer nanomembrane (layer 1 and 2, with thickness of d_1 and d_2) grown on a sacrificial layer is considered. When the sacrificial layer is removed by well-chemical selective etching, part of the nanomembrane is free hanging over a distance h and is initially in an unrelaxed strained state over the whole length L. As the sacrificial layer is gradually being removed, strain-relaxing takes place in the part of the free-hanging bilayer and initiates bending due to the existence of a strain gradient (or Δε) across the bilayer thickness. We suppose that these two layers were subject to biaxial strain ε_1 and ε_2, respectively. Depending on specific materials, these two strains are generally different so that an average strain and a strain gradient can be defined.[33]

$$\varepsilon_{ave} = \eta\varepsilon_1 + (1-\eta)\varepsilon_2$$

$$\Delta\varepsilon = \varepsilon_2 - \varepsilon_1$$

Where $\eta = d_1/(d_1+d_2)$.

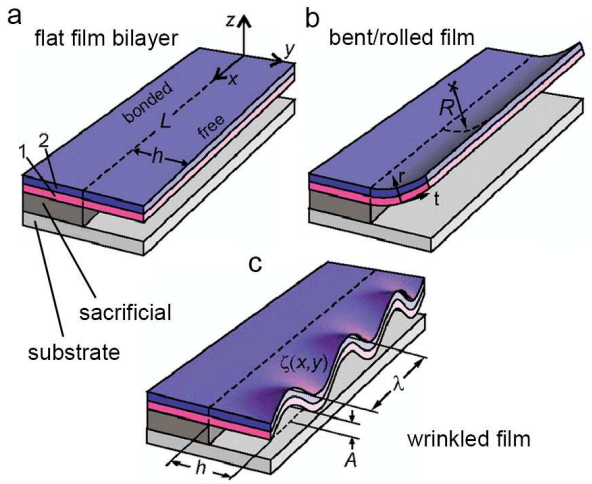

Fig. 2 (Schematics of (a) a flat bi-layer nanomembrane, (b) a bent nanomembrane with radius *R*, and (c) a wrinkled structure. Reprinted with permission from ref. 33. Copyright 2009 American Physical Society.

To determine the bending direction, the length of h is crucial. When h is small, the fixed boundary confinement in the x direction limits the relaxation in x and the strain is relaxed via bending in the y direction (Fig. 2b). With increasing h, the constraint from the fix boundary weakens, thus the membrane stretches in both directions. However, there is still a geometric constraint for strain relaxation in the x direction, thus leading to the formation of wrinkles (Fig. 2c), and the real shape might be a combination of bent and wrinkled structures. [34-36] It should be pointed out that 3D micro-/nanostructures produced by nanomembranes rolling or bending also depend on the strain gradient (or Δε). Wrinkled nanomembranes occur if a relatively small strain gradient exists (Δε < 0.5 %), or rolled nanomembranes are obtained if the strain gradient is large enough (Δε > 0.5 %). In the latter case, the free-hanging bilayer tends to be rolled until the minimized elastic strain energy is achieved, which gives rise to a radius of the curved film as:

$$R_0 = \frac{(d_1 + d_2)^3}{6(1+\nu)d_1 d_2 \Delta\varepsilon}$$

We can clearly see that the self-rolling process is determined by the layer thicknesses (d_1, d_2) and the strain states (ν: Poisson ratio, Δε), which are strongly influenced by film deposition parameters. Meanwhile, Δε>0 implies a roll upwards process, while Δε<0 implies a downwards rolling mechanism. Finally, a tubular nanomembrane can be obtained when the film length is longer than a circumference along the rolling direction.

From above, we know that introduction of a strain gradient perpendicular to the nanomembranes is essential for the fabrication of rolled-up structures. To obtain rolled-up nanomembranes, several methods have been explored. One is utilizing lattice mismatch in nanomembranes grown by epitaxy. Group IV, III-V, and even II-VI semiconductor materials have been successfully strain-engineered and rolled.[37-43] The biggest advantage of this method is that the engineering process is controllable. Due to the well-known values of the lattice constants, we can calculate the strain gradient between the different nanomembranes accurately, which is beneficial to the design of experiments.[44-46] Nevertheless, this method depends on the values of lattice constants, which limits the fabrication of some materials without exact values. Moreover, the epitaxial nanomembranes are expensive and complicated to fabricate, putting severe limits to practical applications. In addition, nanomembranes deposited by other non-epitaxial vapour deposition methods may also be inherently strained containing some built-in stress.[34] The strain gradient can be obtained based on the deposition parameters. Heating or cooling the material system with different coefficients of thermal expansion is another way to generate strain gradients within the nanomembranes.[34]

By combining the two latter approaches, a novel and facile method to roll-up nanomembranes on a polymer sacrificial layer (mainly photoresist) has been explored.[28] Utilizing conventional photolithography, the nanomembranes can be correctly patterned on a photoresist layer during deposition, which provides obvious convenience in accurate positioning of microtubes and module integration on a single chip. It is worth mentioning that the evolution of substrate temperature, deposition rate and the base pressure need to be taken into account during the nanomembrane deposition. Meanwhile, various diameters can be obtained by changing the thickness and the strain gradient of nanomembranes. However, it is not possible to obtain an accurate analytical description of the strain gradient and the diameter of the tubular nanomembrane in such case. In addition, the nanomembranes deposited on photoresist layers are always of poly-crystal or

amorphous nature, which may influence their properties for applications in electronic devices, but may deliver huge potential as electrodes for LIBs due to the amorphous structures. Therefore, the tubular nanomembranes reviewed in this article are mainly fabricated using this method.

2.2 Engineered tubular nanomembranes for lithium-ion batteries

As mentioned above, tubular nanomembranes made by rolled-up nanotechnology can release the strain caused by lithiation or delithiation as well as imply extra interior space for electron and ion transport, thus improving the electrochemical performance for LIBs. For this reason, we have fabricated various kinds of tubular nanomembranes with different architectures using rolled-up nanotechnology and explored their potential applications as high-performance electrodes for LIBs.[47-56] In the following section, we will review the electrochemical performance of these unique architectures containing silicon based, germanium based, and composite tubular nanomembranes and illustrate their inherent merits for use in LIBs.

2.2.1 Silicon based tubular nanomembranes

Silicon (Si) is regarded as one of the most promising anode materials for the next generation LIBs benefiting from its highest theoretical capacity (~ 4200 mAh/ g), environmental benignity, abundance in nature, and low working potential. [57-58] Despite these preeminent properties, conventional Si anodes face significant challenges due to the large volume changes (400 %) during alloy processes to form Li_xSi ($0 \leqslant x \leqslant 4.4$) which hinder Si as a commercial negative electrode because of the loss of electrical contact between active materials caused by mechanical fracture, accumulation of solid-electrolyte interphase layers, and rapid capacity fading during electrochemical cycling.[59] Recently, nanotechnology has achieved a breakthrough to overcome these challenges.[60] Various Si nanomaterials and engineered Si nanostructures such as nanowires/particles, hollow spheres and porous nanostructures have showed stable cycling and high resistance to fracture in spite of the large volume change. [60-63] Besides, composites with carbon such as Si NPs coated with carbon black,[64] carbon-coated yolk-shell structured Si composites,[59] Si-carbon core-shell structures,[65] and even single layer graphene-coated Si nanowires,[66] have been designed to improve the structural and electrical integrity of Si anodes. Different to these works, using engineered 3D tubular nanomembranes, we can not only accommodate the kinetic properties towards Li ion and electron transport, but also minimize the mechanical stress induced by the volume change of Si.

Using a downwards rolling method, Deng et al. have fabricated rolled-up C/Si/C trilayer nanomembranes,[48] where a spin-coated sacrificial layer (photoresist) was firstly deposited on the top of the Si substrate, followed with radio frequency sputtering of C/Si/C multi-layers, during which the intrinsic strain caused by thermal expansion effects was generated. When the sacrificial layer was selectively etched by acetone, the composite nanomembranes naturally peeled off from the Si substrates and broke into micrometer-sized pieces owing to the pulling strain (Fig. 3a), and these pieces further self-rolled into multilayer tubular structures (Fig. 3b). In this unique architecture, Si nanomembranes work as the active layer for Li^+ storage, and the carbon layers serve as the supporting layer because of their high stability and excellent conductivity. As a result, when used as anode for LIBs, the multilayer C/Si/C nanomembranes exhibited synergistic properties and superior electrochemical performance. The tubular C/Si/C multilayers exhibit excellent stability with a highly reversible capacity. The capacity of the 300th cycle is about 1000 mA h/g, almost 100 % of that of the second one at a current density of 500 mA/g (Fig. 3c), such ultra-long cycle life is not observed for most other Si-based anodes. More importantly, the overall tubular morphology as well as the encapsulation of Si layers within the double carbon layers is well maintained even after 82 cycles, revealing the stable cycling performance of the multilayer C/Si/C microtubes for LIBs.

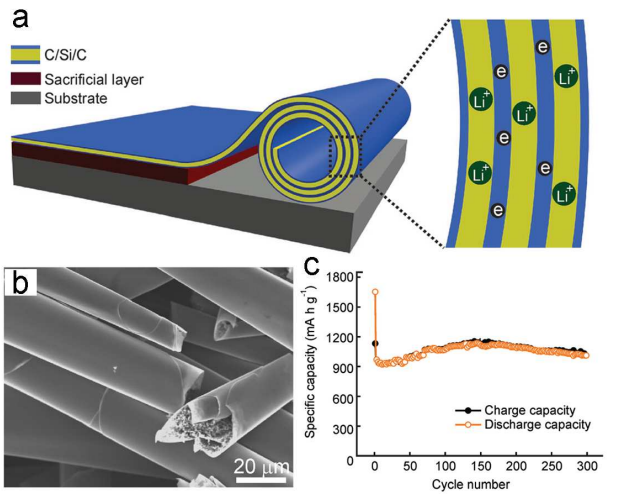

Fig. 3 (a) Fabrication process, (b) SEM image, and (c) cycling performance of the rolled-up C/Si/C multilayer nanomembrances. Reprinted with permission from ref. 48. Copyright 2013 Wiley-VCH Verlag GmbH & Co. KGaA, Weinheim.

Graphene, which consists of single or few stacked ordered sp^2 carbon sheets, has been regarded as an ideal protective material for the electrode materials and has shown great potential in improving battery performance due to its high electrical conductivity and specific surface area. [67] With good flexibility, graphene and rGO are highly compatible with the strain engineering strategy, and have been utilized widely to form composites with other materials to enhance their Li^+ storage performance. To further improve the capacity and cycling stability of Si based tubular nanomembranes, a tubular Si/rGO bilayer nanomembrane consists of parallel aligned Si and rGO nanolayers fabricated using the above rolled-up nanotechnology. [49] The Si/rGO bilayer nanomembranes (Fig. 4a) sandwiched with Si as the electrochemically active layer and rGO as conductive protecting layer are designed to combine the merits of Si nanomembranes and rGO protecting layesr. As expected, the tubular Si/rGO bilayer nanomembranes delivered an initial discharge/charge capacity of 2871/1817 mA h/g with a higher initial Coulombic efficiency of 63.3% at a

current density of 100 mA/g (Fig. 4b), which were much higher than those of the pure Si nanomembranes electrode (2683/1250 mA h/g, 46.6%). Importantly, an ultra-long cycling stability was achieved by using the tubular hybrid bilayer nanomembranes. A high reversible capability of 571 mA h/g was maintained after 2000 charge-discharge cycles at a high current density of 3000 mA/g (Fig. 4c). These results obviously reveal the unique merits of tubular structures combining Si and rGO nanomembranes for releasing the strain generated in the alloy processes and thus realizing high cycling stability.

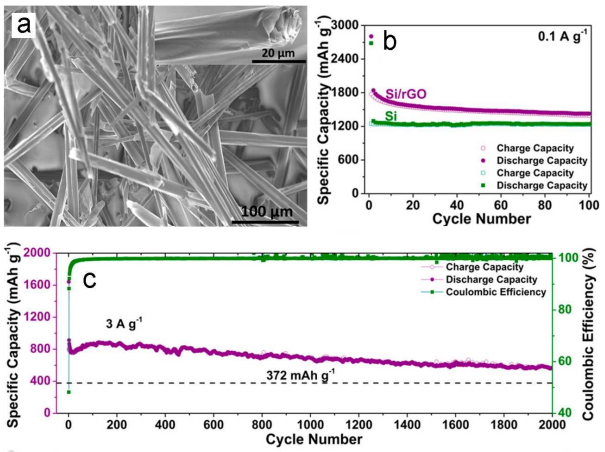

Fig. 4 (a) SEM image of the rolled-up Si/rGO bilayer nanomembranes. (b) Cycling performance at (b) 100 mA/g, and (c) 3 A/g. Reprinted with permission from ref. 49. Copyright 2013 American Chemical Society.

As discussed above, the strain-released rolled-up Si-based nanomembranes do exhibited enhanced capacity and cycling stability. However, in these cases, two or even more different materials were adopted to realize different functionalities for each layer, which not only causes difficulties in the preparation, but also may cause interfacial strain. To solve these problems, Zhang et al. further demonstrated a hierarchical electrode design with just one material. Taking multilayered SiO_x as an example, by controlling the oxygen content x in each SiO_x layer, some desired functionalities for different layers with improved performance can be achieved.[50]

The fabrication process is the same with the rolled-up nanotechnology mentioned above. An oxygen-rich SiO_x (with x ~ 1.85) film and a silicon-rich SiO_y (with y ~ 0.5) film can be obtained by controlling the oxygen partial pressure. Fig 5a shows the morphology of as-fabricated SiO_x/SiO_y tubular structures, and interfaces between the two layers can be clearly observed in Fig. 5b. The outer layer of the membrane is a thin (about 12 nm) oxygen-rich amorphous SiO_x layer, which acts as a strain buffer/ mechanical supporting layer. The inner layer of the membrane is a thicker (about 35 nm) Si-rich amorphous SiO_y layer, which has a large capacity for Li^+ storage provided by the electrochemically active Si domains. The benefits from this unique structure are the first discharge and charge capabilities of 2595 and 1372 mA h/g achieved at 100 mA/g. The specific capacity stabilized at around 1300 mA h/g over 100 cycles, revealing the excellent cycling property caused by the superior mechanical stability. The wound-up layer structure was conserved very well after the first charge and even after 80 cycles (Fig. 5c and 5d), which revealed that the oxygen-rich amorphous SiO_x layer can be an excellent strain buffer layer and the tubular nanomembranes can effectively avoid the mechanical failure during the expansion/contraction of the active layers.

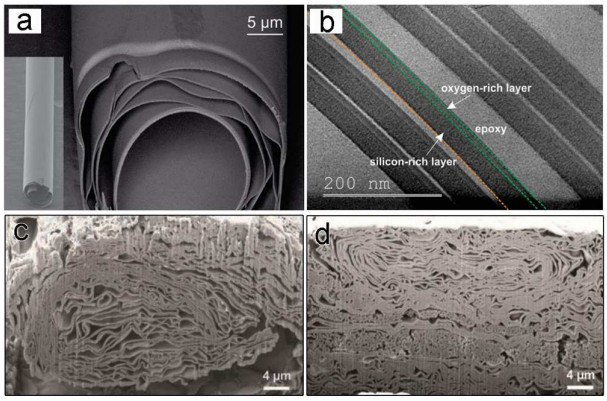

Fig. 5 (a) SEM, and (b) TEM image of SiO_x/SiO_y bilayer nanomembrane. The surface morphology of the cycled electrodes: (c) the first charge, and (d) after 80 cycles. Reprinted with permission from ref. 50. Copyright 2014 Wiley-VCH Verlag GmbH & Co. KGaA, Weinheim.

2.2.2 Germanium based tubular nanomembranes

In addition to Si, germanium (Ge) has also attracted much attention recently because of its high theoretical capacity of 1600 mA h/g despite of its high cost. When compared with Si, Ge has advantages for high-power LIBs because of its intrinsic kinetic superiority. The electrical conductivity of Ge is 10000 times higher than that of Si because of its smaller band gap of 0.6 eV. Besides, the Li^+ diffusion coefficient of Ge is about 400 times higher than that of Si at room temperature.[68-69] Similar to the Si anode, the commercial application of Ge in LIBs is also hindered by the poor cycle stability, because the drastic volume change during the Li^+ uptake and release process results in their pulverization and exfoliation from the current collector, leading to poor cycling ability and rapidly declining capacity.[70] To overcome these problems, tremendous efforts have been made to design materials that can buffer the volume change, including mesoporous Ge particles,[71] Ge nanowires,[72] Ge microcubes,[73] Ge@C nanoparticles,[74] and composite electrodes incorporating graphene.[75-78] Among these electrodes, careful engineering of hybrid Ge-based electrode materials provide both high storage capacity and high conductivity for enhanced Li storage properties.

Using rolled-up nanotechnology, Yan et al. fabricated a new type of configuration based on Ge/Ti hybrid multilayers.[51] Metallic Ti is employed mainly because of its outstanding electrical properties, high chemical stability and mechanical strength to buffer huge volume changes during the lithiation/delithiation processes.[79] Fig. 6a displays the schematic of the fabrication process for the strain release of the Ge/Ti bilayer hybrid films. The Ge/Ti films bent and formed into a tubular structure after etching the sacrificial layer due to

the existing intrinsic stress gradient in the bilayer. The hybrid tubular nanomembranes showed discharge and charge capacities of 1753 and 1490 mA h/g for the first cycle at C/16 (Fig. 6b). Importantly, it is known that the Coulombic efficiency of Ge based anodes is relatively low. However, in our hybrid nanomembranes, a high Coulombic efficiency of 85 % could be achieved (Fig. 6c), which is much higher than that of Ge nanowires (33 %), [80] Ge nanotubes (76 %) [81] and Ge/graphene composites (52 %) [74]. After 100 cycles, the hybrid Ge/Ti microtubes exhibited excellent capacity retention and maintained a stable capacity of about 930 mA h/g with high Coulombic efficiency, demonstrating the advantages of the strain released structures for improving electrochemical properties and enhancing cycling performance.

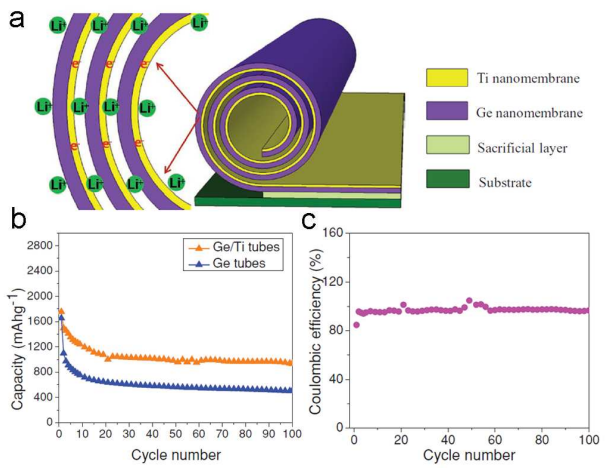

Fig. 6 (a) Schematic illustration, (b) cycling performance, and (c) coulombic efficiency at a current rate of C/16 of the multilater Ge/Ti nanomembranes. Reprinted with permission from ref. 51. Copyright 2013 Wiley-VCH Verlag GmbH & Co. KGaA, Weinheim.

Apart from single phase Ge anodes, Ge-based oxides, such as GeO_2 and GeO_x, were recently found to exhibit significantly better cycling stability and rate capability than pure Ge. The enhanced cycling and rate performance stems from the Ge metal nanocrystals formed by the electrochemical conversion reaction of Ge oxides in the first Li^+ insertion process. [82-86] To further improve the electrochemical properties of Ge-based oxides, composite electrodes containing GeO_x nanostructures and reduced graphene or other carbon materials have been explored. [87-89] Chen et al. has reported a strain drove multilayer graphene/GeO_2 tubular nanomembranes, [52] where GeO_2 multilayers work as the active layers for Li^+ storage, while the graphene serves as the electrically conductive and elastic layer and also as additional lithium storage sites. The SEM image in Fig.7a clearly shows that the layered platelets are composed of curled nanosheets, and the components of a representative tubular graphene/GeO_2 nanomembrane in Fig. 7b are indeed composed of C, Ge and O elements. Such novel graphene-based tubular nanoarchitectures provide short Li^+ pathways and high electrical and ionic conductivity, and hence exhibit much improved specific capacity, super rate capability and cycling performance. As shown in Fig. 7c, the hybrid nanomembranes exhibited excellent rate capability with charge capacities of 886 and 624 mA h/g at 0.2 and 2 C, respectively. Even at a high current of 5 C, capacity of 504 mA h/g was still achieved, much higher than that of the rolled-up pure GeO_2 nanomembranes (239 mA h/g). Remarkably, a highly stable capacity of 571 mA h/g was obtained after 1000 cycles at 2 C, revealing ultra-long cycling life. The enhanced rate capability and cycling stability can be attributed to the highly conductive graphene and shortened diffusion pathway facilitating efficient electron and ion transport, hollow nanostructures with large active surface proving more reaction sites, and strain released nanomembranes favouring cycling stability.

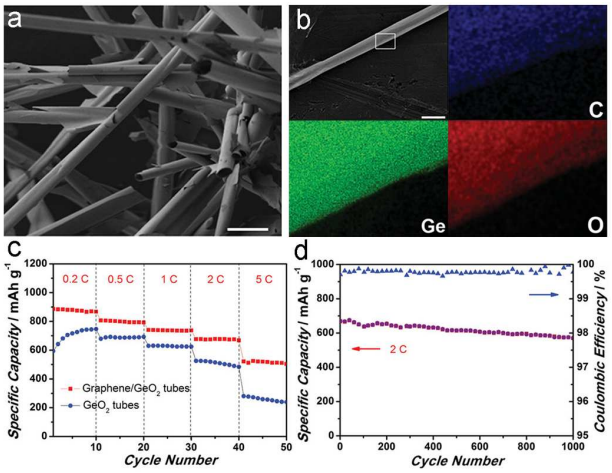

Fig. 7 (a) SEM image, (b) elemental mapping images, (c) rate, and (d) long cycling performance of the graphene/GeO_2 tubular nanomembranes, scale bar: 20 μm. Reprinted with permission from ref. 52. Copyright 2013 Wiley-VCH Verlag GmbH & Co. KGaA, Weinheim.

2.2.3 Other tubular nanomembranes

Rolled-up nanotechnology is highly adaptable for self-curled tubular structures, and many other self-wound nanomembranes have also been fabricated to explore their applications in improving the Li^+ storage performance. For examples, RuO_2/C composite tubular nanomembranes showed enhanced cycling stability when compared with that of RuO_2 power. [47] The discharge capacity of the RuO_2 powder was reduced to 90 mA h/g after 15 discharge cycles at C/16, while the RuO_2/C tubular nanomembranes still showed a discharge capacity of 830 mA h/g with a Coulombic efficiency of 99%, implying enhanced lifetime and good reversibility of the hybrid tubes. The improved electrochemical properties can be ascribed to the tubular nanomembrane structure allowing for strain-relax, and the stable supporting carbon layer maintaining the electrode integrity during the conversion reaction of the active layer. Moreover, the large electron contact area and good adherence caused by the close contact between the whole active layer and the conductive carbon layer are also beneficial for the improved electrochemical performance.

As one of the transition metal oxides, NiO has been considered as a promising anode material for next-generation LIBs due to its high theoretical capacity (718 mA h/g), low cost, and improved safety.[90-92] Apart from this, the density of NiO is 6.67 g/cm^3, leading to high volumetric energy density. [93] Till now, NiO nanosheets, [94] nanorod arrays, [95] microtubes, [96] and NiO/C composites, [97-99] have been explored to obtain high specific capacities with average cycling stability. However, none of them realize super rate capability and long cycling stability because of the intrinsic low conductivity and drastic volume variation during lithiation or delithiation.

To this end, Sun et al. have designed 3D "curved" NiO nanomembranes by using the typical rolled-up method followed by a thermal oxidation process.[53] The product is composed of large quantities of curved nanomembranes with an average diameter around 10 μm (Fig. 8a). This particular structure results in excellent lithium storage performance as it combines efficient 3D electron transport, excellent connectivity with electronic and ionic sources, and short diffusion distance. As expected, the tubular nanomembranes exhibited excellent rate capability, even after cycling at an extremely high C-rate of 50 C, the capacity is able to recover to the initial value when the current rate is set back to 0.2 C after 110 cycles. Importantly, the "curved" NiO electrode showed ultra-long cycle life for LIBs. The electrodes deliver a high capacity of 721 mA h/g at 1.5 C (1 C = 718 mA/g) after 1400 cycles with excellent stability (Fig. 8b). Such impressive superior power rate and ultra-long lifespan for NiO-based electrodes are the best results ever reported.

Using the tubular nanomembranes construction, the strain of lithiation/delithiation in SnO_2 electrodes can also be relieved. The result showed that a long cycling life of 1000 cycles at 1600 mA/g with a high reversible capacity of 854 mA h/g could be realized using rolled-up amorphous SnO_2 nanomembranes. It is worth mentioning that the amorphous electrode can deliver a high rate capability up to 40 A/g, which is greatly improved over most of the pure SnO_2 anodes. [54] Such superior performance is ascribed to the structural advantages of amorphous structures, such as the short diffusion paths for Li^+, and high efficiency to accommodate the strain benefited from the amorphous structure.[100-101] Moreover, the unique mechanical feature also enables the electrodes to buffer the strain delaying pulverization and extending the cycling life.

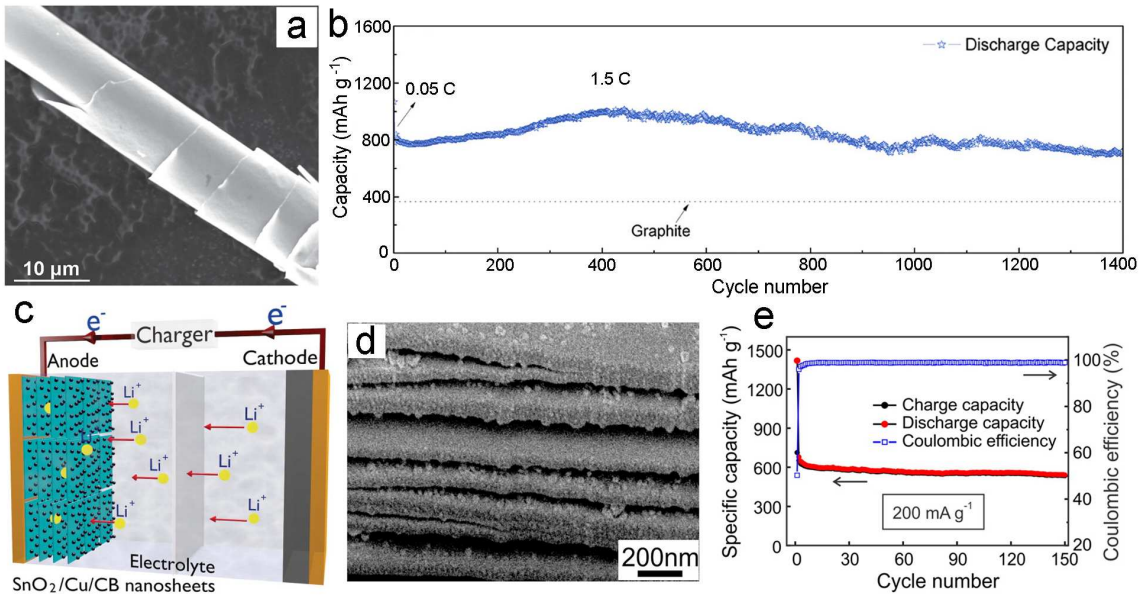

Fig. 8 (a) SEM image, and (b) reversible capacity versus cycle number of the curved NiO nanomembranes. Reprinted with permission from ref. 53. Copyright 2014 Wiley-VCH Verlag GmbH & Co. KGaA, Weinheim. (c) schematic configuration of a stacked SnO_2/Cu cell. (d) SEM image (d) cycling performance of the SnO_2/Cu nanosheets. Reprinted with permission from ref. 55. Copyright 2013 American Chemical Society.

As reviewed above, the rolled-up tubular nanomembranes can efficiently improve the electrochemical performances of LIBs. The main drawback of the tubular nanomembranes is the large hollow center though it can benefit the ion transport. To some extent, the hollow structure limits the packing density and therefore the potential for further practical applications. To increase the volume energy of tubular nanomembranes, compact sandwich-like nanosheet stacks were also created by applying rolled-up nanotechnology and a subsequent compression step.[55] To obtain the sandwich-like structures, SnO_2/Cu bilayered tubular nanomembranes are firstly strain engineered with carbon black (CB) periodically clamped between each layer. Then, compact 2D nanosheet stacks with well-defined channels can be readily formed after compressing the rolled-up tubular nanomembranes with a pressure around 2.9 kPa (Fig. 8d). With CB acting as the inter layer, restacking and agglomeration of the SnO_2/Cu sandwich-like structures can be prevented during charge/discharge processes, and volume changes can also be accommodated by the free channels (Fig. 8c). Besides, these 2D nanosheets possess large

active surfaces, enhancing the electrochemical reactions at the interface between active materials and the electrolyte. Furthermore, the hybrid Cu thin films can act as a conductive layer providing excellent electronic conductivity and a structural buffer preserving the integrity of the whole electrode. Benefiting from these unique advantages, the 2D sandwich-like SnO_2/Cu hybrid anodes thus exhibited a high reversible capacity of 713 mA h/g and a stable cycling performance of about 75% capacity retention at 0.2 A/g after 150 cycles (Fig. 8e).

2.3 Tubular nanomembranes for Li-O_2 batteries

Rechargeable Li-O_2 batteries have gained recognition as one of the most promising candidates to replace conventional LIBs because of the possibility to achieve high energy density desired for long-range operating electric vehicles.[102-104] However, key limitations, such as large charge/discharge overpotential, low rate capability, and poor cycle life, must be resolved for practical applications. A desirable Li-O_2 cathode must be conductive, stable in extremely oxidative environment, and show good catalytic activity towards both oxygen reduction reaction (ORR) and oxygen evolution reaction (OER).[105-107] Therefore, the oxygen electrode should consist of porous conductive substrates to accommodate insoluble discharge products because the overall energy density is determined by the amount of insoluble discharge products stored in the oxygen electrode.[108] Besides, the oxygen electrode should facilitate oxygen diffusion and electrolyte impregnation. So it is essential to optimize the porosity of the oxygen electrode to provide large space for insoluble discharge products and enhance oxygen diffusion and electrolyte impregnation throughout the electrode.

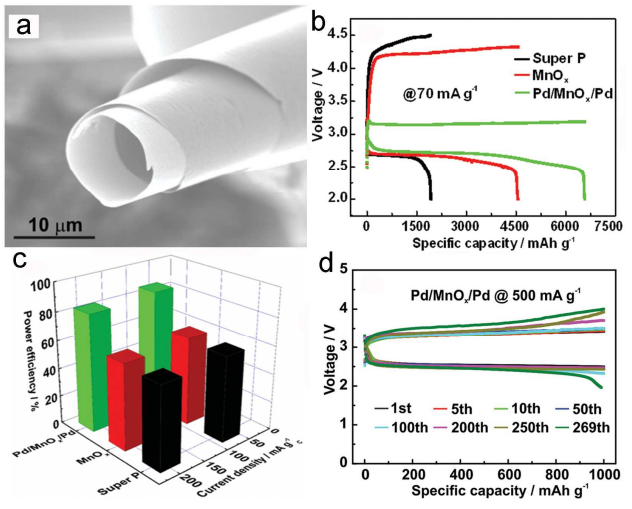

Fig. 9 (a) SEM image of the Pd/MnO_x/Pd nanomembrane. (b) Voltage profiles, (c) Power efficiencies, and (d) cycling stability of the hybrid nanomembranes. Reprinted with permission from ref. 56. Copyright 2015 Wiley-VCH Verlag GmbH & Co. KGaA, Weinheim.

To our delight, the hollow architecture of rolled-up tubular nanomembranes renders them the very candidate for the oxygen electrode. Very recently, Lu et al. fabricated a trilayer Pd/MnO_x/Pd nanomembrane (Fig. 9a) by using the typical rolled-up nanotechnology.[56] When used as the cathode catalyst, a specific capacity of 6750 mA h/g can be achieved at a current density of 70 mA/g (Fig. 9b), much higher than that of Super P (1930 mA h/g) and pure MnO_x nanomembranes (4500 mA h/g). More importantly, by sandwiching the MnO_x layer between two ultrathin Pd films, the charge overpotential was significantly lowered to only about 3.16 V (the overpotential is about 0.2 V, which is the theoretical limit proposed in the literature[109]), leading to a power efficiency of about 86%. When the current density increases to 200 mA/g, the power efficiency of Pd/MnO_x/Pd still stays over 80%, much higher than that of bare MnO_x and Super P (Fig. 9c). The cathode catalyst also exhibited high cycling stability. As revealed in Fig. 9d, there is no apparent degradation of both the discharge and charge potentials up to 190 cycles for the battery with the Pd/MnO_x/Pd electrode and it finally cycles 269 times before the discharge voltage drops to 2.0 V, which shows a great improvement over previously reported data in the literature. Moreover, the terminal charge potential of Pd/MnO_x/Pd electrode stays below 4.2 V in the whole process, effectively suppressing the side reactions and achieving stable cycling performance.

2.4 Electrochemical fundamental study based on single rolled-up nanomembrane tube batteries

Rolled-up nanotechnology offers an advanced strategy to deterministically rearrange 2D plane nanomembranes into 3D micro/nano-hierarchical tubes. Importantly, combined with conventional photolithography, the 3D micro/nano tubular nanomembranes can be easily patterned on a chip, which shows great potential to fabricate miniature devices especially energy storage devices for exploring the kinetics of ion or electron storage fundamentally. In this section, we will summarize several interesting works on the fundamental studies of single tubular nanomembranes based LIBs, SCs and electrostatic capacitors.

2.4.1 Single tubular LIBs

The above results have demonstrated that the tubular nanomembranes can greatly enhance the electrochemical performance for lithium ion storage due to the fast ionic transport and powerful strain accommodation benefiting from the unique hollow micro/nano-hierarchical structure. Despite these achievements, a deeper understanding of the relationship between the tubular structure, electrical/ionic conductivity, the electrochemical kinetics as well as the lithium storage performance still needs to be explored. However, it is a great challenge to obtain this information with batteries based on bulk electrodes, because they are often composed of electrodes, conductive additives and polymer binders, which will bring some uncertainties into the fundamental electrochemical kinetic studies. To eliminate these uncertain facts, the investigation based on a single active material is a must.

Till now, considerable efforts have been made to develop such platforms using single active material with well-defined

geometry, which enables direct observation of the electrochemical behaviors and the structural changes of the active materials. Based on the studies of single nanostructure devices, lithographic techniques were developed and applied to battery researches. Through fabricating a microelectrode attached to the particle to establish an electrical contact, Uchida's group investigated the kinetics of Li^+ extraction/insertion by measuring the current and potential of a single particle. [11] An electrode platform to test the electrical transport and observe the structural evolution of single silicon nanowires has also been investigated.[111] Recently, combining single nanostructure device diagnostics with in situ electron microscopy techniques, much understanding of battery operational processes have been deeply studied. Huang et al. directly observed the lithiation of a single SnO_2 nanowire during electrochemical charging by using in situ transmission electron microscopy.[112] Using the same method, Wang and co-workers presented a two-phase process of electrochemical lithiation in amorphous Si.[113] MacDowell have also investigated the electronic properties and structural changes in a single Si nanowire.[114] However, these technologies showed here are too complicated to be operated, and depends largely on the equipments, which may not allow widely for the direct correlation of the electrochemical property with the structure on the same single electrode material. Rolled-up nanotechnology, by contrast, is much readily accessible, flexible, and cost-effective, and is very convenient to place the tubular structure accurately on a chip. Therefore, it is expected that the rolled-up nanotechnology can be a practical method to fabricate on-chip energy storage devices to learn the direct relationship between electrical transport, structure and electrochemistry of single electrode.

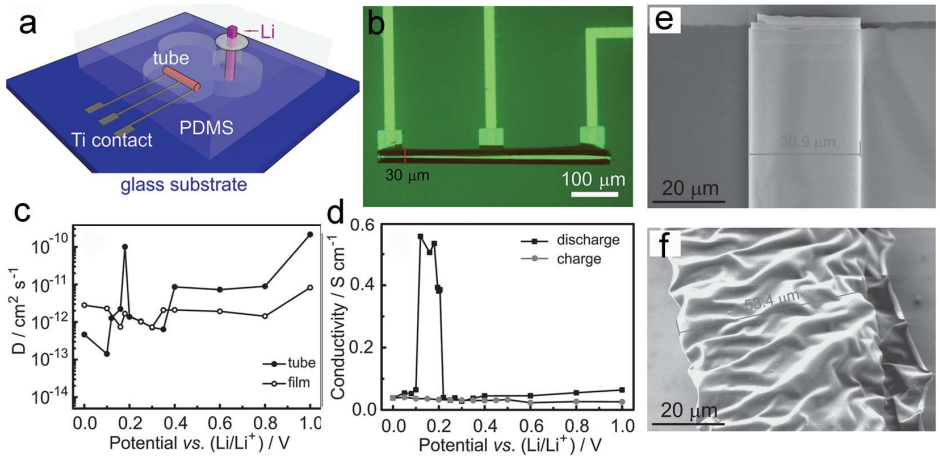

Fig. 10 (a) Schematic illustration of the single device. (b) Optical microscopy image of a single rolled-up silicon tube. (c) Diffusion coefficient of Li^+ ion in Si tube. (d) Electrochemical conductivity during first discharge/charge cycle. Morphology of a tube before cycling (e) and after three cycles. Reprinted with permission from ref. 115. Copyright 2014 Wiley-VCH Verlag GmbH & Co. KGaA, Weinheim.

Using the rolled-up nanotechnology, Si et al. have presented a lab-on-chip electrochemical device platform to probe the electrochemical kinetics, electrical properties and lithium driven structural changes.[115] Fig. 10a shows a schematic of a micro-LIB based on a single Si tubular nanomembrane, where a single Si tube and a strip of lithium foil were used as working electrode and counter electrode, respectively, combined with a polydimethylsiloxane (PDMS) chamber as electrolytic cell. Fig. 10b reveals an optical microscopy image of the single rolled-up Si tubular nanomembrane with a diameter of around 30 μm, and three Ti contacts were made with one in the middle of the tube and two at its two ends. The biggest advantage of this approach to fabricate the on-chip device is that the tubular nanomembranes is self-wound at the end of the Ti electrodes by controlling the experiment parameters. Using the single rolled-up tube platform, we have gained a better understanding of the different diffusion behavior of Li^+ in the Si tubular nanomembrane. As demonstrated in Fig. 10c, the maximum diffusion coefficient occurs at around 0.2 V, probably due to the increased contact area between the electrode and electrolyte because the fast reaction between Li and Si introduces a large volume expansion as well as the formation of wrinkles and small particles on the surface. The Li^+ diffusion coefficient in the Si tube is about 10^{-11} cm^2/s, which is several times higher than that in planar Si films under all potentials except at 0 V. The maximum conductivity of 0.56 S/cm occurs at around 0.12 V, which can be attributed to the decomposition of the conductive alloy and the formation of the less-conductive alloy (Fig. 10d). Meanwhile, the volume expansion of the Si tube upon the insertion of lithium contributes to the increase of the overall conductivity, since the cross section increases during the expansion of the tube. Furthermore, the morphology evolution of a single Si tube can be easily observed in our device. The single Si tube reveals a smooth surface (Fig. 10e), while after three cycles, the tube exhibits a highly wrinkled structure (Fig. 10f) with apparently accommodating large volume strains introduced during electrochemical processes.

Using the single-microtube-based LIB device, the direct correlation of the electrical transport and electrochemistry properties of the hybrid multilayer Ge/Ti microtubes for Li^+ storage was also probed.[51] The device starts with the

fabrication of a plane strained multilayer nanomembrane by the sequential deposition of Ge and Ti thin films on top of a sacrificial layer (Fig. 11a). Once the sacrificial layer is selectively removed, the strained Ge/Ti bilayer starts to roll towards the Au finger structures. After the rolling process, the microtube on top of the Au fingers established an electrical connection (Fig. 11b). Figure 11c shows a single rolled-up device for electric transport measurements during lithiation and delithiation. The middle electrode acts as the anode for the lithium-ion battery and the two electrodes at the open ends are used for electrical transport measurements. Using the single rolled-up Ge/Ti microtube as the working electrode, propylene carbonate/ethylene carbonate as the electrolyte, and a metallic lithium foil as the counter electrode, we have conducted an electrical transport investigation of a single Ge/Ti microtube before and after lithiation. Firstly, the hybrid Ge/Ti structure exhibits a much higher electric conductivity compared to that of the pure Ge microtube (Fig. 11d), highlighting the merits of the incorporation of the Ti multilayer in significantly improving the conductivity. After lithiation, an enhancement of the conductivity performance by almost one order of magnitude can be observed due to the insertion of lithium into the amorphous Ge microtubes and the formation of more conductive Li_xGe alloys (Fig. 11e). Meanwhile, after delithiation, a decrease in the conductivity was measured and the conductivity of the hybrid Ge/Ti can be partially recovered (Fig. 11f), which is attributed to the decomposition of the conductive Li_xGe alloy and the formation of the less conductive Ge.

The strain-release method provides a straightforward and novel way to explore the fundamental transport characteristic of lithium ion and conductivity evolution during the reaction, while overcoming limitations apparent in conventional lithography. It is known that the insertion rate of Li^+ in active electrode varies from site to site. To further understand the diffusion kinetics of Li^+ in the single tubular electrodes of batteries, multi-contacts on single tubular electrode may be designed for recording the conductance of different parts of the electrode at the charge/discharge status and giving detailed information. For example, Mai's group explored the Li^+ and Na^+ transport in different parts of single $H_2V_3O_8$ nanowire by using on-chip micro electrochemical devices.[116] To push forward the fundamental and practical research of tubular electrode materials for energy storage applications, fundamental studies on this area might be an exciting motivation.

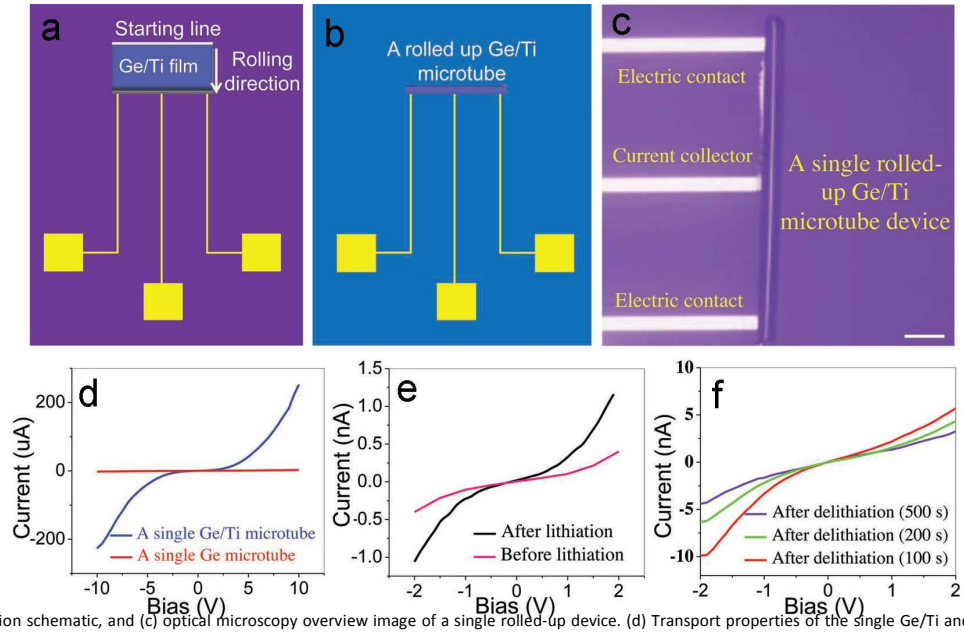

Fig. 11 (a, b) Fabrication schematic, and (c) optical microscopy overview image of a single rolled-up device. (d) Transport properties of the single Ge/Ti and Ge microtubes. (e, f) Transport properties of the single Ge/Ti microtubes before and after discharge. Reprinted with permission from ref. 51. Copyright 2013 Wiley-VCH Verlag GmbH & Co. KGaA, Weinheim.

2.4.2 Single tubular supercapacitors

Rolled-up nanotechnology has shown great opportunities towards lab-on-chip electrochemical device platform based on individual tube micro/nanostructures. Apart from the single tubular LIBs for the electrochemical kinetics reviewed above, on-chip single tubular supercapacitors for different proton diffusion behavior have also been carefully designed. Ji et al. have demonstrated a single Swiss roll redox micro-SC by rolling up a multilayered Au/RuO_2 nanomembrane.[117] The prepared Swiss roll microtubes is approximately 7 μm in diameter with around 7 windings deduced from the rolling length of 150 μm. The on-chip tubular SC revealed clear electrochemical reversibility of the Faradaic redox transition of amorphous RuO_2. The calculated capacitance is about 1 μF at scan rate of 100 mV/s, corresponding to 2200 $\mu F/cm^2$, which is close to that of the theoretical redox capacitance of anhydrous RuO_2.

It is worth to mention that the micro-SC size is greatly reduced when compared with a commercial 1 μF capacitor, and the 2D area is reduced to 1/20 of that of the unrolled planar film. The other merit of this rolled-up tubular SC is that the proton diffusion behavior of the redox micro-device can be tuned readily by controlling the hollow core, the multilayer rolled-up wall, the tube diameter and rotation.

It is known that micro-SCs have been studied greatly in the last several years. However, little attention has been paid on the electrochemical kinetics of single active material because there is no mature platform. Excitingly, the self-rolled-up single tubular SCs reviwed here exhibited great potential for studying charge transfer at the electrolyte/electrode interface. Furthermore, this technique can also be further applied to electrochemical microprobes in cell electrophysiology and local detection of microenvironments.

2.4.3 Single tubular capacitors

In the case of miniaturized energy autonomous systems (MEAS) containing electronic devices, energy harvesters and energy-storage elements, such as wireless sensor networks and medical device implants, the reduction of the whole system must be addressed. To make energy storage devices suitable for MEAS, several features are needed, containing long life (10 years or more), short charging times (seconds to minutes), ultra-long charge-discharge life (up to 10 000 cycles), small geometrical dimensions (< 1 mm^2), high temperature stability, and parallel manufacturing capability. [118] Alternatively, electrostatic capacitors can fulfil very well those criterias including life and charging time, charging-discharging cycles, miniaturization and large scale production. Therefore, electrostatic capacitors become more appealing for MEAS when the footprint area is reduced.

The rolled-up nanomembranes offer a feasible route toward reducing the footprint by curling thin membranes into tubular architectures. Bufon et al. have fabricated self-wound ultracompact capacitors (UCCap) by using the rolled-up nanotechnology.[32] As outlined in Fig. 12 a-c, the process starts with the fabrication of a planar strained multilayer nanomembrane by the sequential deposition of metal and dielectric thin films on top of a sacrificial layer. The 3D UCCap is self-assembled by selectively removing the sacrificial layer. The rolling of the tubular nanomembrane capacitor shown in Fig. 12d results in the reduction of the footprint to about 0.002 mm^2, which signifies a compactification of 25 times of the original unrolled size (0.050 mm^2). It is worth mentioning that the specific capacitance of the UCCap can be easily changed by adjusting the number of windings. For example, the capacitance per footprint area significantly increases from 1.3 to 200 μF/cm^2 with enhanced winding number (Fig. 12e), revealing the merit of combing top-down with self-assembly methods. Startlingly, the UCCap by rolling a nanomembrane with length of 1 mm exhibited a high power density of 2000 W/kg and a specific energy density of 0.55 Wh/kg in the range of supercapacitors, confirming the huge potential to improve the performance by reducing the footprint area using the rolled-up nanomembranes.

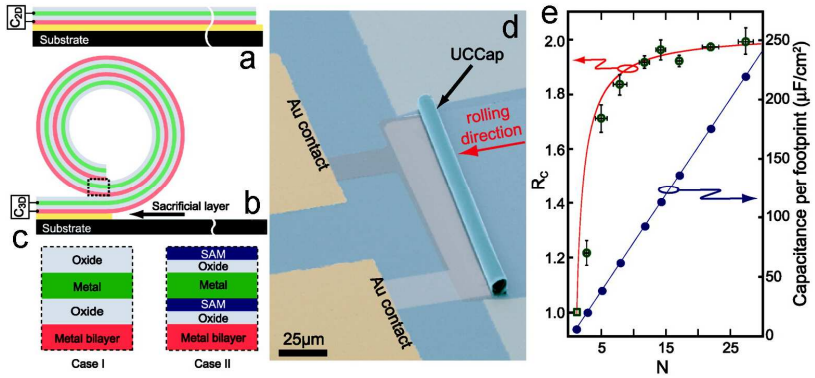

Fig. 12 (a, b) Layer sequence to create rolled-up capacitors. (c) Layer sequence for inorganic and hybrid organic/inorganic capacitors. (e) Relationship between capacitance per footprint area and number if winding. Reprinted with permission from ref. 32. Copyright 2010 American Chemical Society.

As confirmed above, the self-assembling rolled-up process is responsible for the decrease of the device's footprint area and consequently for the increase of the capacitance per footprint area. To further increase the capacitance, Sharma et al. tailored the electrical properties by combining different high-k dielectrics, such as Al_2O_3, TiO_2 and HfO_2. [119] Fig. 13a shows the sketch of a roll-up UCCap and the corresponding oxide layer sequence used to form the device, in which the electron beam evaporated Au/Ti and Cr membranes served as the two capacitor plates with a multi-layer stack dielectric consisting of Al_2O_3, TiO_2 and HfO_2 between them. As expected, the capacitances of rolled-up capacitors based on 100 % Al_2O_3 dielectric layers as well as Al_2O_3-TiO_2 multilayers increase by a factor of about 1.3. Upon HfO_2 incorporation, an increase of typically 1.7 is observed upon rolling. Figure 13b shows the increase of capacitances for rolled-up devices as a function of the amount of incorporated HfO_2 and TiO_2. The incorporation of high-k oxides allows achieving an increase of up to 100 % of capacitance when compared to UCCaps using only Al_2O_3 as dielectric. Apart from tailoring the capacitance of UCCaps by incorporating HfO_2 and TiO_2, the devices can also be properly engineered in a variety of configurations to allow increased

capacitance and other applications. For example, we can fabricate UCCaps with longer tubes and consequently larger active areas. Besides, the technology demonstrated here also allows creating self-rolled double-tube capacitors electrically connected in parallel. Fig. 13c demonstrates a 4-inch wafer containing 1600 devices, where two UCCaps are electrically contacted in parallel and share the same bond pads (Fig. 13d). This novel double-tube design satisfies the required architecture for electrically driven autonomous systems.[120] Furthermore, two parallel contacted UCCaps can also be obtained by a double rolling process (Fig. 13e) where two complete sacrificial/capacitor layer stacks are processed on top of each other and then rolled in parallel. UCCaps with different geometries can be easily fabricated demonstrating the high flexibility of the rolled-up fabrication process.

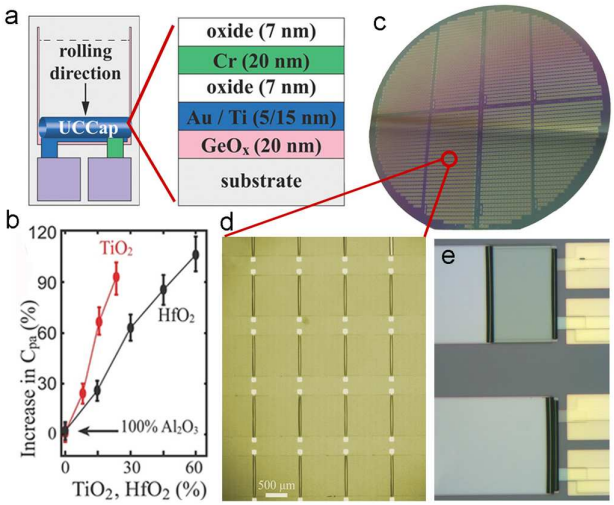

Fig. 13 (a) Rolling up and layer sequence of the UCCap. (b) Capacitance per footprint area, Cpa, and increase of Cpa for UCCaps as a function of the HfO_2 and TiO_2 incorporation. (c) 4-inch Si/SiO_2 wafer containing array of double tube UCCaps (d). (e) UCCaps processed in parallel. Reprinted with permission from ref. 119. Copyright 2014 Wiley-VCH Verlag GmbH & Co. KGaA, Weinheim.

3. Thinning nanomembranes

2D plane nanomembranes have lateral dimension at least two orders of magnitude larger than the thickness and can well combine the merits of the 0D and 1D counterparts. [121] With the unique mechanical feature, the 2D nanomembranes can be distorted, wrinkled and folded into 3D configurations, which is attractive and expected to buffer the strain of lithiation/delithiation for the applications in LIBs. [122] On the other hand, the nanomembranes can also provide 2D transport pathways between the layers, which can promote pseudocapacitive type electrodes for fast charge and discharge. [123] Recently, numerous inorganic nanomembranes have been designed as electrodes for energy storage devices with the aim of improving their electrochemical properties. In this section, we will give a brief summarise on the recent development of 2D nanomembranes utilized as electrodes for LIBs and SCs with a focus on metal oxide, graphene and their composites.

3.1 Thin nanomembranes for lithium-ion batteries

Transition-metal oxides such as Co_3O_4,[124] Fe_2O_3,[125] and NiO[126] have been widely studied as anode materials for rechargeable LIBs owing to their potentially higher specific capacities than that of graphite. Unfortunately, these metal oxides exhibit low reversible capacity, unsatisfactory capacity retention and poor rate capability. As mentioned above, 2D nanomembranes possess high mechanical stability and short ion transport pathways, which can be used to achieve long cycling life and high rate capability with satisfactory reversible capacity. For example, Liu et al. have designed free-standing Fe_2O_3 nanomembranes, which exhibited very encouraging results with ultra-long cycling life and high rate capability.[127] The Fe_2O_3 nanomembranes with thickness of 103 - 165 nm (Fig.14a) were obtained by annealing oxidation of Fe nanomembranes in air. Benefiting from the unique 2D structure, the nanomembranes exhibited excellent rate performance. As shown in Fig. 14b, the reversible capacity of the last cycle at 0.5 C, 1 C, 2 C, 5 C, 10 C, 20C, and 50 C in the first turn was 822, 750, 668, 552, 462, 354, and 178 mA h/g, respectively. Importantly, ultra-long cycling performance can also be achieved using the film-like electrodes (Fig. 14c). The initial discharge/charge capacity at 1 C was 1232/803 mA h/g and the reversible capacity of the 100 th cycle at 1 C is 834 mA h/g. When the current density increases to 6 C, the first discharge/charge capacity was 715/610 mA h/g. Then the electrode kept an ultra-long and stable cycling at 6 C with reversible capacity of about 570 mA h/g. The reversible capacity of 530 mA h/g after 3000 cycles was still much higher than the theoretical capacity of graphite.

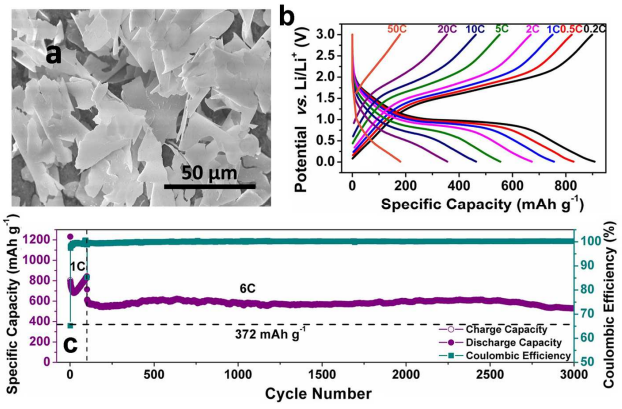

Fig. 14 (a) SEM image, (b) rate capability, and (c) cycling performance of the Fe_2O_3 nanomembrane electrodes. Reprinted with permission from ref. 127. Copyright 2001, Nature Publishing Group.

Hybrid nanostructures have been proposed to surpass the limitations associated with single phased nanomaterials.[128] Recently, it has been demonstrated that the presence of an active metal (Fe, Ni, Co, etc.) phase enhances the electric conductivity and facilitates the electrochemical reaction

kinetics of electrode materials. [129-130] Based on these considerations, Sun et al. have designed and synthesized novel multifunctional Ni/NiO hybrid nanomembranes with rough and undulating surface morphologies by a physical deposition method combined with chemical etching and thermal oxidation.[131] The ratio of NiO to Ni was determined to be 52.4 : 47.6 wt %. The freestanding thin nanomembranes delivered initial discharge and charge capacities of 857 and 588 mA h/g at 0.1 C (1 C = 718mA/g), respectively. After 900 cycles at 6 C, the capacity can remain at about 743 mA h/g with a high Coulombic efficiency. More importantly, the anodes can be discharged and charged at an ultrahigh rate of 115 C if only the mass of NiO is taken into calculation or 60 C if the total mass of Ni/NiO nanomembranes is considered.

Using a similar construction, Yu et al. also demonstrated 3D Au/a-Ge thin nanomembranes by depositing amorphous Ge into nanoporous gold films. [132] The hybrid electrode delivered a reversible capacity as high as 1200 mA h/g and showed outstanding capacity retention of 90 % after 100 cycles when tested for Li storage in the voltage window 0.005 - 1.2 V (vs. Li^+/Li). In addition, this material preserved 47.5 % of its 1 C capacity when cycled at 60 C. The super electrochemical properties can be attributed to the specific bicontinuous structure of the Au/Ge electrode, which provides an interconnected electrolyte-filled pore-network that enables rapid ion transport. Besides, the use of a-Ge preformed in the Au structure is able to avoid the solid-state amorphization. Furthermore, the 3D porous Au network provides highly conductive electron transport pathways, and the specific 3D porous structure offers enough space to permit charge-discharge volume changes, which can prevent isolation even after long cycle lifetimes.

Designing hybrid carbon-based nanomembranes is another appealing strategy to improve the reaction kinetics and realize superior energy storage performance of the metal oxide nano-films. Among various carbon nanomaterials, graphene has been accepted as a leading candidate for hybrid electrodes due to its superlative electronic properties, large surface area, and excellent flexibility. [133] For the hybrid graphene based electrodes, the dispersed active materials attached on graphene sheets can provide a large surface area for Li^+ access and effectively shorten the diffusion pathway for Li^+ transport. To realize excellent performance of the hybrid graphene based electrodes, the intimate interaction between graphene and active materials is highly desired to enhance effective and rapid charge transfer and prevent volume change and aggregation of nanoparticles upon cycling.[134]

Yu's group have demonstrated 2D $ZnMn_2O_4$-graphene nanosheets by a facile two-step synthesis approach involving a polyol process followed by thermal annealing.[135] As revealed in Fig. 15 a-b, conductive graphene nanosheets act as flexible 2D substrate for uniform anchoring of $ZnMn_2O_4$ nanoparticles. The graphene sheets can provide elastic buffer space to accommodate volume changes of $ZnMn_2O_4$ nanoparticles during charge/discharge processes, thus leading to good cycling stability. Furthermore, the graphene sheets have good electric conductivity and can serve as electron transport channels for $ZnMn_2O_4$ nanoparticles, thus facilitating effective charge transport for high rate performance. Moreover, unique 2D hybrid nanostructures can enable large active sites for Li^+ transport for higher specific capacity. When compared with $ZnMn_2O_4$ nanoparticles and $ZnMn_2O_4$-rGO mixture, the hybrid nanosheets delivered enhanced rate capability at current densities from 200 to 3200 mA/g (Fig. 15c). Moreover, the hybrid nanomembranes also showed long cycling stability. After 1500 cycles, a stable discharge capacity of 650 mA h/g could still be obtained, resulting in a capacity retention of 81 % (Fig. 15d). Using the $ZnMn_2O_4$-graphene nanosheets as anode and $LiFePO_4$ nanosheets as cathode, the full battery delivered a reversible capacity of 124 mA h/g after 100 charge-discharge cycles at 30 mA/g over a voltage range of 0.9 - 3.9 V vs. Li^+/Li, corresponding to 94 % capacity retention.[136]

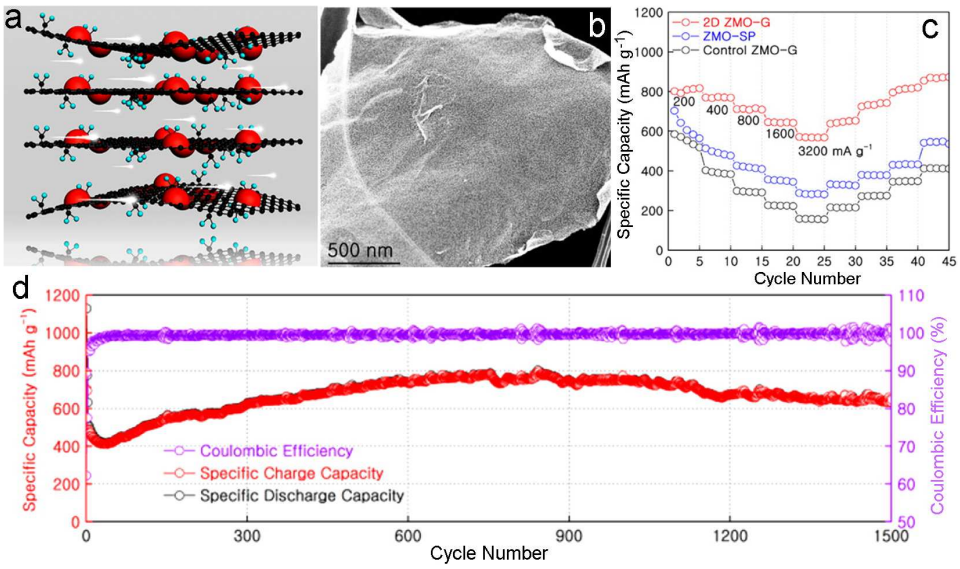

Fig. 15 (a) Schematic illustration, (b) SEM image, (c) rate performance and (d) long cycling stability of the 2D hybrid $ZnMn_2O_4$/grapheme nanostructure. Reprinted with permission from ref. 135. Copyright 2014 American Chemical Society.

3.2 Thin nanomembranes for supercapacitors

As mentioned above, thin nanomembranes exhibit high mechanical stability, which possess great potential applications in electronic devices that could be bent and stretched for future electronics. Furthermore, highly transparent devices can also be realized by using thin nanomembranes. In recent years, many thin nanomembranes have been designed to achieve flexible, transparent, and miniature SCs. In this section, we review the recent development of thin nanomembranes towards micro-SCs with a focus on their flexibility, transparency, and micro-volume.

3.2.1 Graphene nanomembranes

Graphene nanomembranes are expected to play a crucial role in the development of electrodes for SCs owing to their large in-plane conductivities. The use of ultrathin graphene films has the following advantages: substantial mechanical strength of the graphene materials allows for the formation of flexible and robust thin films that can be used for graphene-based flexible and stretchable SCs. The transparency of the graphene film in SCs allows for application in transparent electronics.

Recently, many meaningful works on graphene nanomembranes based SCs have been reported which exhibited high flexibility, stretchability, and transparency. For example, Chen's group have prepared ultrathin graphene films with thicknesses of 25, 50, 75, and 100 nm by using a vacuum filtration method.[137] After transfer onto a PET substrate, the highest transmittance of approximately 70 % can be obtained for a 25 nm thick grapheme film at 550 nm. The conductivities of the films range from 800 – 1000 S/m. Besides, the film collected on a PET substrate can be readily bent to some degree without losing conductivity. When used as electrodes for SCs, capacitances of 111, 105, 102, and 99 F/g were obtained for the 25, 50, 75, and 100 nm films at a scan rate of 10 mV/s, respectively. To pursuit transparent and stretchable SCs, Dai's group demonstrated a wrinkled graphene sheet with a large area (2*4 cm^2) by chemical vapor deposition (CVD) of methane with the carrier gas of argon and hydrogen under 1000 ^oC.[138] The wrinkled graphene sheet was then transferred with its structural integrity onto a PDMS substrate to exhibit high transparency of 50 – 60 % at 550 nm (94 % transmittance for the 0.5 mm thick PDMS substrate) and excellent stretchability. Using PVA-H_3PO_4 as gel electrolyte, the planar SCs showed optical transmittances in the range of 48 to 57 %. Furthermore, their CVs and charging-discharging performance as well as their specific capacitance were almost unchanged when they were stretched up to 40 % strain, revealing excellent stretchability of the graphene-based SCs.

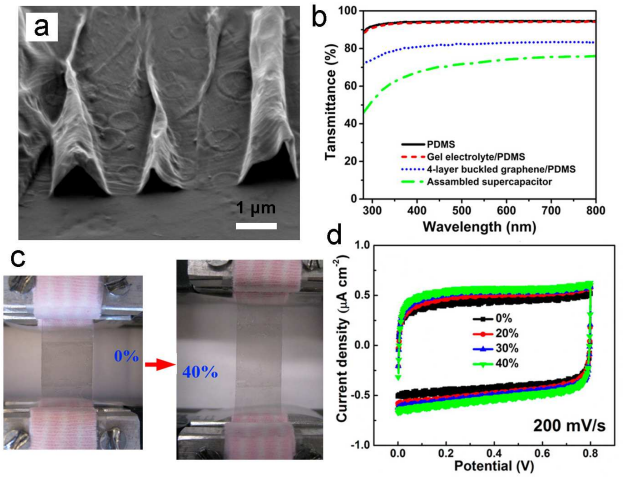

Fig. 16 (a) SEM image of the buckled graphene film. (b) Transmittances of the supercapacitor. (c) Digital photo of the supercapacitor stretched from the tensile strain of 0% to 40%. (d) CV curves at different tensile strains. Reprinted with permission from ref. 139. Copyright 2014 American Chemical Society.

Using the prestraining-then-buckling method, Xu et al. have also realized the stretchability of graphene electrodes SCs with high transparency and high rate.[139] Four-layer graphene films were processed by fabricating individual graphene films, followed by a film transporting and laying-up process. Fig. 16a shows the morphology of the buckled graphene layer with nanoscale, ripple-like features. After assembled into a SC based on the graphene/PDMS film using PVA-H_2SO_4 gel electrolyte, an optical transmittance of 72.9 % can be obtained at a wavelength of 550 nm (Fig. 16b). In addition, the as-assembled SC was also capable to withstand tensile strains of up to 40 % (Fig. 16c). The area specific capacitances increased with the tensile strains from 0 % to 40 % (Fig. 16d), which can be attributed to the increased pressure applied by the upper and lower PDMS films during stretching by 20 %, 30 %, and 40 %, that can facilitate the wettability of the graphene electrode. Importantly, CV curves maintained an ideal, rectangular shape at scan rates of up to 6000 mV/s at 0 % and 4000 mV/s at 40 %, respectively, indicating good electrical double-layer capacitive behavior and rate capability.

The above-discussed transparent graphene nanomembranes are usually coated on a transparent substrate. However, transparency for the freestanding flexible graphene paper has never been realized, because a thin transparent graphene sheet will fracture easily when the template or substrate is removed using traditional methods. So, it is a great challenge to fabricate freestanding transparent graphene nanofilms with good flexibility, electrical conductivity to use in multifunctional electronics. Very recently, Li et al. have solved the problem and have presented a freestanding, flexible and transparent graphene paper.[140] In their preparation, graphene paper was fabricated from a sample of NaCl power in a microwave plasma-enhanced CVD system. After the fabrication, the

interconnected graphene structure can be mechanically peeled off using a sharp razor blade. The peeled-off freestanding graphene paper showed excellent transmittance (Fig. 17a) and comprised regularly arranged prismlike graphene microstructures (Fig. 17b). To fabricate transparent and flexible SCs, the graphene film on PDMS was then prepared by spreading the H_2SO_4/HNO_3 treated graphene sheet onto a PDMS substrate followed by a drop of alcohol to eliminate the wrinkles and fix the active material. After assembled with PVA-H_2SO_4 gel electrolyte, the as-prepared SC with 380 nm thickness of graphene delivered a transmittance of about 46.5 % at a wavelength of 550 nm (Fig. 17c). The specific capacitance was calculated to be 3.3 mF/cm^2, which was nearly 1000 times greater than that of the laminated/wrinkled ultrathin CVD graphene film-based SC and at least ten times greater than those of the previously reported transparent and flexible SCs based on pure carbon materials.[139, 141-142] When the device was stretched to different strains, the capacitance remained nearly constant, demonstrating its relatively good stretchability for practical applications. A potential of 2.0 V can be realized by connecting two SCs in series, which could light up a light-emitting diode (LED, with a turn-on voltage of 1.5 V), demonstrating the potential applications of flexible and transparent graphene nanomembranes based SCs (Fig. 17d).

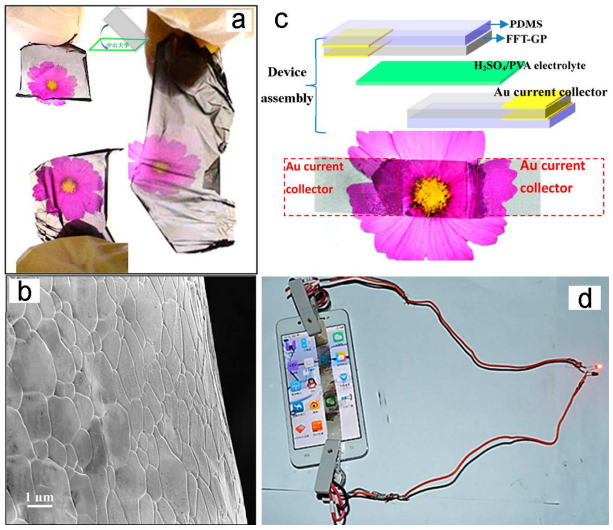

Fig. 17 (a) Photographs, and (b) SEM image of a grapheme paper. (c) Fabrication and photograph of a transparent supercapacitor. (d) Power delivery of supercapacitors in series. Reprinted with permission from ref. 140. Copyright 2015 American Chemical Society.

3.2.2 Hybrid nanomembranes

To push the energy and power density limit of thin SCs based on nanomembranes, a great deal of effort has been devoted to improving the capacitance by fabricating composited nanomembrane electrodes. Particularly, composites consist of carbon materials and pseudocapacitive materials such as MnO_2,[143] RuO_2,[144] and other metal oxide[145] are the most promising electrode materials for film SCs. This kind of composites can effectively take advantage of both the high conductivity of the carbon materials and the high specific capacitance of the pseudocapacitive materials, and hence result in significant improvements in both the energy density and the power density.

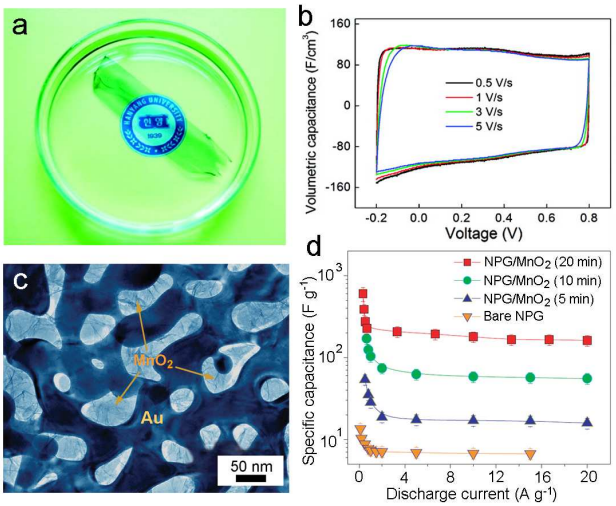

Fig. 18 (a) Photo image of a PEDOT/CNS hybrid nanomembrane. (b) CV curves of supercapacitor. Reprinted with permission from ref. 147. Copyright 2012 American Chemical Society. (c) SEM image of the Au/MnO_2 film. (d) Specific capacitance of the supercapacitor. Reprinted with permission from ref. 151. Copyright 2011, Macmillan Publishers Limited.

In addition to the carbon materials/metal oxide composites, recently, composite nanomembranes combining carbon with conductive polymers such as polyaniline (PANI), poly(3,4-ethylenedioxythiophene) (PEDOT), and polypyrrole (PPy), have been studied extensively for energy storage.[146] For example, Lee et al. developed a mechanically robust, electrically conductive, freestanding, and transparent hybrid nanomembrane. The hybrid structure was made of densified carbon nanotube sheets (CNS) that were coated with PEDOT by using vapor phase polymerization. Hybrid nanomembranes peeled from the glass slide were optically transparent and freestanding in ethanol (Fig. 18a). The one-layer CNS/85 wt % PEDOT nanofilm exhibited a transmittance of 56 % at 550 nm and a sheet resistance of 312 Ω/sq. When used as electrode for SC in a three-electrode cell, the hybrid nanomembranes showed rectangular cyclic CV curves even at high scan rates of up to 5 V/s (Fig. 18b). With a scan rate going from 0.01 to 100 mV/s, the volumetric capacitances were 123 and 40 F/cm^3. As calculated, the hybrid nanomembrane exhibited a power density of 7910 W/cm^3 (4391 kW/kg) and energy density of 70 mWh/cm^3 (37 Wh/kg). The gravimetric energy density of the hybrid nanomembrane was almost twice that of the transparent graphene nanofilm (thickness = 50 nm) SC and the power density was at least 130 times higher.[137]

In the past few years, printable SCs have been advanced through fabrication of thin films, which have exhibited excellent scalability and flexibility.[148-149] Very recently, using graphene-conducting polymer hybrid nanomembranes as electrodes, Müllen's group demonstrated an ultrathin

printable SC with alternating current (AC) line-filtering performance.[150] In their method, the conductive hybrid ink of electrochemically exfoliated graphene and poly(3,4-ethylenedioxythiophene): poly(styrenesulfonate) (PEDOT:PSS) was spray-coated on a gold-deposited 2.5-μm-thick PET substrate with a tuneable thickness ranging from nanometers to micrometers. Then ultrathin printable SC were constructed with two hybrid nanomembranes sandwiching a thin polymer gel electrolyte of PVA/H_2SO_4 and exhibited an unprecedented volumetric capacitance of 348 F/cm^3 and excellent cycling stability with no capacitance loss after 50 000 cycles.

As mentioned above, the presence of an active metal phase can enhance the electric conductivity and facilitate the electrochemical reaction kinetics of electrode materials. Composite nanomembranes combining metal phase and metal oxides have also been investigated to improve the electrochemical performance of planar SCs. In 2011, Chen's group presented a 100-nm-thick nanoporous gold/MnO_2 composite nanofilm (Fig. 18c). The hybrid nanofilm was fabricated by de-alloying $Ag_{65}Au_{35}$ (at %) to produce conductive nanoporous gold and then plating nanocrystalline MnO_2 into the nanopores.[151] When used as active electrodes for a simple SC in a 2 M Li_2SO_4 aqueous solution, the specific capacitances of nanoporous hybrid nanofilms at various currents appeared to be much higher than those of the bare nanoporous gold, and a longer plating time (up to 20 min) for the MnO_2 yielded the highest specific capacitances (Fig. 18d). The power and energy densities of the SC reached maxima of 57 Wh/kg and 16 kW/kg, respectively, with a MnO_2 plating time of 20 min. The high energy density greatly exceeds the values of commercial devices at the same power density.[152]

3.3.3 Thin nanomembranes for on-chip supercapacitors

Developing miniaturized SCs, also called micro-SCs, has attracted much attention in recent years for powering microelectronics, because the conventional SCs are too large for very small devices and conventional manufacturing methods are not compatible with microelectronic fabrication.[153] For the micro-SCs, the most important performance metrics are the high area energy and power density due to the small footprint area of the devices. Despite the micro-SCs with planar 2D electrodes discussed above, in-plane on-chip SCs have been designed for further enhancing the area energy and power density, in which each electrode consists of several fingers. The electrode fabrication usually follows the thin film fabrication methods with the addition of an electrode-patterning step before or after electrode deposition. Till now, many on-chip SCs have been fabricated based on various active electrodes such as monolithic carbon films,[154] OLC micrometer-thick layer,[155] PANI nanowire arrays,[156] MoS_2 films,[157] and so on.

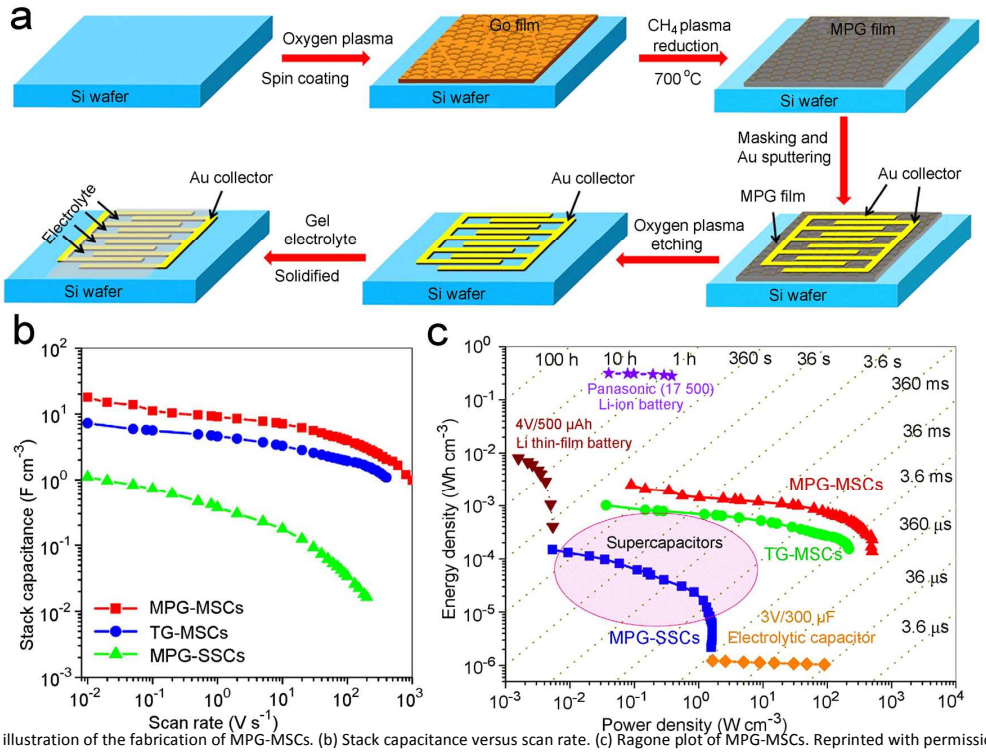

Fig. 19 (a) Schematic illustration of the fabrication of MPG-MSCs. (b) Stack capacitance versus scan rate. (c) Ragone plot of MPG-MSCs. Reprinted with permission from ref. 162. Copyright 2013, Macmillan Publishers Limited.

An alternative way to increase the energy density of micro-SCs is using high surface area graphene as the electrode material.[158-159] The thickness of these graphene films are usually at the micro scale. It is known that an increase in the thickness of the electrode and mass loading of the electrode material increases the electrode resistance and results in

decreased gravimetric capacitance. [160] Therefore, making graphene films on a nanoscale have been pursued for high-performance on-chip SCs. Niu et al. achieved a flexible, compact, ultrathin, and all-solid-state on-chip SC based on lateral ultrathin rGO interdigitated microelectrodes, which were fabricated by using photolithography as well as selective electrophoretic buildup. [161] The specific capacitances of the on-chip SC based on rGO interdigitated electrodes (25 nm thickness) were much higher than those of the plane SC on 2D rGO film electrodes due to the shortened diffusion path lengths. The calculated volumetric energy density is 31.9 mWh/cm^3 and the maximum volumetric power density is 324 W/cm^3.

To further improve the rate performance of on-chip SCs, Wu et al. developed a novel class of all solid-state in-plane interdigital micro-SC based on methane plasma reduced graphene (denoted MPG) films with a nanoscale thickness of 6 - 100 nm.[162] Fig. 19a shows the fabrication process of the in-plane micro-SC, where PVA-H_2SO_4 was used as the gel electrolyte. Due to the high electrical conductivity (345 S/cm) of the MPG films and the planar geometry of the micro-devices, the resulting micro-SC delivered a maximum areal capacitance and a stack capacitance of 17.9 F/cm^3. When compared with the MPG film-based planner SC and TG film-based in-plane micro-SC, the MPG film based in-plane micro-SC showed enhanced rate capability (Fig. 19b) even charged and discharged rapidly up to 1000 V/s, three orders of magnitude higher than conventional SCs, highlighting the superiority of the planar device geometry over the classical sandwich-like stack geometry for SCs. As excepted, the micro-SC manifested an ultrahigh power density of 495 W/cm^3 which is at least 50 times higher than that of conventional SCs. An energy density of 2.5 mWh/cm^3, that is comparable to lithium thin-film batteries, could also be achieved (Fig. 19c). In addition, the micro-SC could deliver a superior cycling stability (98.3% capacitance retention after 100 000 cycles at an ultrahigh scan rate of 50 V/s).

Graphene quantum dots (GQDs), which are assembled by single or few layer graphene with a tiny size of only several nanometers, have attracted tremendous research interest due to their unique properties associated with both graphene and QDs. [163] Resulting from the high specific surface area, good electrical conductivity and high mobility, GQDs are one idea electrode material for on-chip SCs to improve the capacity and rate performance. Using a simple electro-deposition approach, Liu et al. demonstrated a GQDs//GQDs symmetric micro-SC with interdigital structure fabricated from GQDs thin-film with thickness of 312 nm.[164] The as-made GQDs micro-SC had excellent power response with very short relaxation time constant and excellent cycle stability. Importantly, the on-chip SC delivered superior rate capability up to 1000 V/s without any CV curve variance, revealing a fast charge transfer in the bulk of the GQDs and a small equivalent series resistance (ESR) of the micro-SC. The excellent electrochemical performance can be attributed to the larger specific surface area, more surface active sites, and more accessible edges, which conveniently afford ample interfaces for the fully accessible of ion adsorption/desorption and the excellent electron mobility.

Because of having higher energy and power densities than carbon materials in aqueous electrolytes, metal oxides have been explored as a kind of electrode material for SCs. Among numerous metal oxides, MnO_2 is considered to be a most attractive candidate as electrode material for SCs because of its abundant natural resources, low-cost, environmental friendliness, and high specific capacitance.[165] However, the low ionic and electrical conductivity of pristine MnO_2 often leads to poor rate performance. For micro-SCs, the short electrolyte diffusion distance should enable high rate capability of MnO_2 electrodes. For example, Wang et al. presented a two-step lithography fabrication method to realize on-chip micro-SC based on nanostructured MnO_2 micro-electrode arrays with a narrow interelectrode distance of 4 μm. [166] This micro-SC device exhibited a high areal capacitance of 56.3 mF/cm^2 at a current density of 27.2 μA/cm^2 and an energy density of 5.01 mW h/cm^2 at a power density of 12.02 mW/cm^2.

To further improve the electrochemical performance of manganese oxide based mirco-SCs, Si et al. have designed MnO_x/Au multilayer thinfilms on flexible polyethylene terephthalate (PET) substrates. The hybrid membranes were deposited by electron beam evaporation for use in on-chip micro-SCs, in which very thin layers of gold were incorporated into the MnO_x layer as conductive additives to enable effective charge transport and electrode integrity, thus endowing the electrodes with high capacity, high rate capability and excellent cycling stability. [167] Each finger has a length of 4.8 mm, a width of 100 μm, and an interelectrode distance of 100 μm with a 50 nm-thick MnO_x/Au multi-layered film (Fig. 20 a-b). Due to the unique structure, the multi-layered nanofilm exhibited a volumetric capacitance of about 78.6 F/cm^3 at a scan rate of 10 mV/s, much higher than that of the bare MnO_x nanomembrane (Fig. 20c). The micro-SC exhibits a maximum energy density of 1.75 mW h/cm^3 and a maximum power density of 3.44 W/cm^3. Furthermore, good long-term cycling stability, with a capacitance retention rate of 74.1 % after a large cycling number of 15 000 times was also achieved, demonstrating the high stability of the on-chip micro-SC based on the composite nanomembranes.

Journal Name

ARTICLE

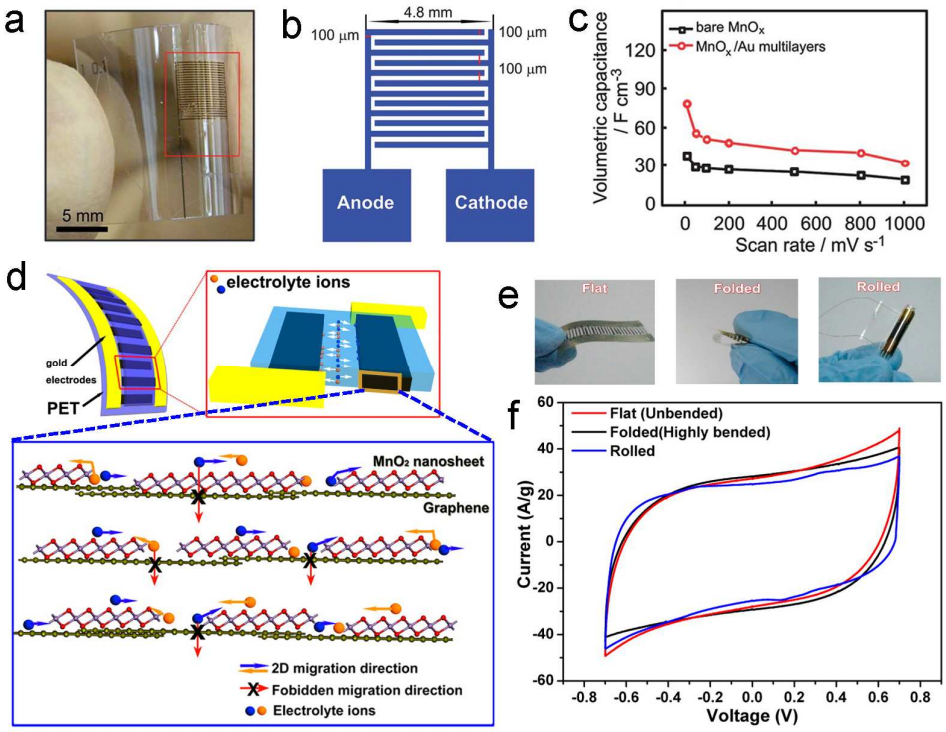

Fig. 20 (a) Photograph of a real, flexible micro-supercapacitor. (b) Schematic diagram of the symmetric microsupercapacitor with 24-interdigital fingers. (c) Volumetric capacitance for MnO_x/Au multilayers and bare MnO_x micro-supercapacitors. Reprinted with permission from ref. 167. Copyright 2013, The Royal Society of Chemistry. (d) Design of hybrid 2D δ-MnO_2/graphene structures based planar supercapacitors. (f) CV curves for the planar supercapacitor under three different bending states: (e) flat, folded, and rolled. Reprinted with permission from ref. 168. Copyright 2013, American Chemical Society.

One problem of the multi-layered nanomembranes is that the layer-by-layer tight stacking in the thin film form inevitably diminishes the interlayer space between ultrathin nanosheets, which could significantly hinder the electrolyte ion diffusion. To this end, Peng et al. presented a novel hybrid structure by integrating δ-MnO_2 nanosheets on graphene sheets to enhance performance of on-chip micro-SCs greatly. [168] As revealed in Fig. 20d, the hybrid structures could introduce more electrochemically active surfaces for absorption/desorption of the electrolyte ions and create extra interface area at the hybrid interlayer to facilitate charge transport during charging/ discharging processes, offering good rate capability and cycling stability. In addition, the integrated δ-MnO_2 nanosheets serving as active centers for the pseudocapacitive reactions contributed to the great enhancement of the specific capacitance. Meanwhile, the δ-MnO_2 integrated on graphene could potentially tailor the distance between each sheet of densely stacked graphene and open up the interlayer space to allow more electrolyte ions to penetrate efficiently into the hybridized film. Accordingly, the as-fabricated in-plane SC based on the hybrid film with thickness of 50 nm yielded high specific capacitances of 254, 249, 232, 217, and 208 F/g at current densities of 0.5, 1, 2, 5, and 10 A/g, respectively, and delivered a high energy density of 17 Wh/kg at a power density of 2520 W/kg, which was superior to graphene based planar SCs. Meanwhile, the in-plane micro-SC also exhibited excellent flexibility without noticeable structural destruction and performance degradation even after being folded or rolled thousands of times (Fig. 20 e-f), demonstrating a significant feature of the next-generation flexible energy storage devices.

Conclusions and outlook

This review summarizes some representative applications of engineered nanomembranes with a focus on tubular nanomembranes and plane nanomembranes for lithium ion batteries, lithium-O_2 batteries, capacitors, and

supercapacitors. As illustrated in this paper, nanomembranes have proven to be effective in improving the performance of these devices due to their novel geometrical characteristics and unique machinability. The rational and creative design of unique structures of nanomembranes helps to address the significant issues encountered during the electrochemical reactions, thus dramatically enhancing the capacity, rate capability, and cycling life of nanomembranes electrodes. In general, nanomembranes improve in performance by (i) providing a large surface area to boost the electrochemical reaction or ion adsorption occurring at the interface between electrodes and electrolyte, (ii) shortening the ion and electron transport paths to ensure the fast reaction, thus enhancing the rate performance, (iii) enabling hybrid electrodes to deliver high energy and power densities by applying merits of different materials, (iv) engineering into various architectures to achieve high flexibility, excellent stretchability and super transparency for micro-electronic devices. These developments reviewed in this article greatly enrich engineered nanomembranes as effective electrodes and represent promising steps towards viable energy storage devices. However, though the merits of engineered nanomembranes have been well demonstrated as high performance electrodes, there are still several aspects of nanomembranes that need to be addressed.

(i) More attempts on next generation energy storage devices based on tubular nanomembranes are needed. Till now, application of nanomembranes in energy storage devices mainly focus on lithium ion batteries, which have demonstrated enhanced electrochemical performance. Based on these achievements, lithium-sulfur batteries, lithium-O_2 batteries, sodium-ion batteries, etc. should be studied extensively to explore the high feasibility of the unique tubular nanomembranes, and improve the specific capacity, rate capability, and cycling stability of these devices.

(ii) Deeper and broader understanding of lithium storage mechanisms and electrochemical reaction pathways for a single tubular nanomembrane should be generated. *In-situ* nanocharacterization techniques have recently been utilized to analyze lithium storage mechanisms in several cell models with complicated fabrication processes. As the rolled-up nanotechnology delivers unique advantages for fabricating microbatteries using single tubular nanomembranes, clear observations of morphology evolution and conductivity changes are expected to be easily achieved. In addition, lithium ion insertion/deinsertion and electron transport at different parts of a single tube can be explored to obtain deeper understanding of lithium ion diffusion and electron transport.

(iii) Fundamental studies on all-solid-state on-chip supercapacitors based on single tubular nanomembranes should attract more interest for future miniature electronic devices. Although single tubular nanomembrane based electrostatic capacitors and capacitor arrays wer realized, the storage energy needs to improve to power miniature electronic devices for practical applications. To this end, single tubular micro-supercapacitors and device arrays with high energy may make the miniature electronic devices possible to use in our daily life.

(iv) Planar nanomembranes for micro-integrated energy systems are undoubtedly a promising research area. In this integrated energy system, energy collection and energy storage, combined with other electronic devices are realized with one device. Resulting from excellent mechanical stability, high flexibility, and good machinability of the 2D plane nanomembranes, flexible and wearable integrated micro-energy systems might not be far off.

Acknowledgements

We acknowledge the support from the "Thousand Talents Program", the Natural Science Foundation of Jiangsu Province of China (no. BK20140315), the National Natural Science Foundation of China (no. 51402202), key laboratory of advanced carbon materials and wearable energy technology in Suzhou, Jiangsu Shuangchuang Plan, and the Priority Academic Program Development of Jiangsu Higher Education Institutions (PAPD).

Notes and references

1 B. Dunn, H. Kamath and J. M. Tarascon, *Science*, 2011, **334**, 928-935.
2 M. Armand and J. M. Tarascon, *Nature*, 2008, **451**, 652-657.
3 P. G. Bruce, S. A. Freunberger, L. J. Hardwick and J. M. Tarascon, *Nat. Mater.*, 2012, **11**, 19-29.
4 S. J. Guo, S. J. Dong, *Chem. Soc. Rev.*, 2011, **40**, 2644-2672.
5 G. N. Zhu, Y. G. Wang and Y. Y. Xia, *Energy Environ. Sci.*, 2012, **5**, 6652-6667.
6 C. M. Park, J. H. Kim, H. Kim and H. J. Sohn, *Chem. Soc. Rev.*, 2010, **39**, 3115-3141.
7 X. Wang, B. Liu, Q. Xiang, Q. Wang, X. Hou, D. Chen and G. Shen, *ChemSusChem*, 2014, **7**, 308-313.
8 X. Wang, B. Liu, X. Hou, Q. Wang, D. Chen and G. Shen, *Nano Res.*, 2014, **7**, 1073-1082.
9 X. Wang, Q. Xiang, B. Liu, L. Wang, T. Luo, D. Chen and G. Shen, *Sci. Rep.*, 2013, 2007.
10 X. B. Chen, C. Li, M. Gratzel, R. Kostecki and S. S. Mao, *Chem. Soc. Rev.*, 2012, **41**, 7909-7937.
11 Y. Yang, G. Y. Zheng and Y. Cui, *Chem. Soc. Rev.*, 2013, **42**, 3018-3032.
12 Q. F. Zhang, E. Uchaker, S. L. Candelaria and G. Z. Cao, *Chem. Soc. Rev.*, 2013, **42**, 3127-3171.
13 H. L. Wang and H. J. Dai, *Chem. Soc. Rev.*, 2013, **42**, 3088-3113.
14 X. Wang, K. Jiang and G. Shen, *Mater. Today*, 2015, **18**, 265-272.
15 J. H. Liu, J. S. Chen, X. F. Wei, X. W. Lou and X. W. Liu, *Adv. Mater.,* 2011, **23**, 998–1002.
16 J. H. Liu and X. W. Liu, *Adv. Mater.*, 2012, **24**, 4097-4111.
17 M. Choi, K. Na, J. Kim, Y. Sakamoto, O. Terasaki and R. Ryoo, *Nature*, 2009, **461**, 246-249.
18 A. K. Geim, *Science*, 2009, **324**, 1530-1534.
19 S. Y. Yin, Y. Y. Zhang, J. H. Kong, C. J. Zou, C. M. Li, X. H. Lu, J. Ma, F. Y. C. Boey and X. D. Chen, *ACS Nano*, 2011, **5**, 3831-3838.
20 M. Kaempgen, C. K. Chan, J. Ma, Y. Cui and G. Gruner, *Nano Lett.*, 2009, **9**, 1872-1876.
21 X. Peng, L. Peng, C. Wu and Y. Xie, *Chem. Soc. Rev.*, 2014, **43**, 3303-3323.

22 J. Feng, X. Sun, C. Wu, L. Peng, C. Lin, S. Hu, J. Yang and Y. Xie, *J. American Chem. Soc.*, 2011, **133**, 17832-17838.
23 C. Zhang, H, Yin, m. Han, Z. Dai, H. Pang, Y. Zheng, Y. Q. Lan, J. Bao and J. Zhu, *ACS Nano*, 2014, **8**, 3761-3770.
24 W. Liu, C. Lu, X. Wang, R. Y. Tay and B. K. Tay, *ACS Nano*, 2015, **9**, 1528-1542.
25 Y. Mei, G. Huang, A. A. Solovev, E. B. Urena, I. Mönch, F. Ding, T. Reindl, R. K. Fu, P. K. Chu and O. G. Schmidt, *Adv. Mater.*, 2008, **20**, 4085-4090.
26 P. Poizot, S. Laruelle, S. Grugeon, L. Dupont and J. M. Tarascon, *Nature*, 2000, **407**, 496-499.
27 X.-L. Wang, W.-Q. Han, H. Chen, J. Bai, T. A. Tyson, X.-Q. Yu, X.-J. Wang and X.-Q. Yang, *J. Am. Chem. Soc.*, 2011, **133**, 20692-20695.
28 O. G. Schmidt and K. Eberl, *Nature*, 2001, **410**, 168.
29 D. Grimm, C. C. B. Bufon, C. Deneke, P. Atkinson, D. J. Thurmer, F. Schäffel, S. Gorantla, A. Bachmatiuk and O. G. Schmidt, *Nano Lett.*, 2013, **13**, 213−218.
30 V. Magdanz, S. Sanchez and O. G. Schmidt, *Adv. Mater.*, 2013, **25**, 6581-6588.
31 A. Madani, M. Kleinert, D. Stolarek, L. Zimmermann, L. Ma and O. G. Schmidt, *Optic. Lett.*, 2014, **39**, 189-192.
32 C. C. B. Bufon, J. D. C. González, D. J. Thurmer, D. Grimm, M. Bauer and O. G. Schmidt, *Nano Lett.*, 2010, **10**, 2506-2510.
33 P. Cendula, S. Kiravittaya, Y. Mei, C. Deneke and O.G. Schmidt. *Physical Review B*, 2009, **79**, 085429.
34 M. H. Huang, F. Cavallo, F. Liu and M. G. Lagally, *Nanoscale,* 2011, **3**, 96-120.
35 W.-P. Huang, H. H. Cheng, A. I. Fedorchenko, A.-B. Wang, *Appl. Phys. Lett.*, 2007, **91**, 053103.
36 R. Huang and Z. Suo, *J. Appl. Phys.*, 2002, **91**, 1135-1142.
37 F. Cavallo, R. Songmuang, C. Ulrich and O. G. Schmidt, *Appl. Phys.Lett.*, 2007, **90**, 193120.
38 N. Y. Jin-Phillipp, J. Thomas, M. Kelsch, Ch. Deneke, R. Somuang and O. G. Schmidt, *Appl. Phys. Lett.*, 2006, **88**, 033113.
39 R. Somuang, A. Rastelli, S. Mendach and O. G. Schmidt, *Appl. Phys. Lett.*, 2007, **90**, 091905.
40 M. H. Huang, C. Boone, M. Roberts, D. E. Savage, M. G. Lagally, N. Shaji, H. Qin, R. H. Blick, J. A. Nairn and F. Liu, *Adv. Mater.*, 2005, **17**, 2860-2864.
41 D. J. Thurmer, Ch. Deneke, Y. F. Mei and O. G. Schmidt, *Appl. Phys. Lett.*, 2006, **89**, 223507.
42 P. O. Vaccaro and K. Kubota, T. Aida, *Appl. Phys. Lett.*, 2001, **78**, 2852-2854.
43 J. Q. Hu, Y. Bando, J. H. Zhan, M. Y. Liao, D. Golberg, X. L. Yuan and T. Sekiguchi, *Appl. Phys. Lett.*, 2005, **87**, 113107.
44 F. Liu, M. G. Lagally and J. Zang, *MRS Bull.*, 2009, **34**, 190-195.
45 S. V. Golod, V. Ya. Prinz, V. I. Mashanov, A. K. Gutakovsky, *Semicond. Sci. Technol.*, 2001, **16**, 181-185.
46 G. Huang and Y. Mei, *Adv. Mater.*, 2012, **24**, 2517-2546.
47 H.-X. Ji, X.-L. Wu, L.-Z. Fan, C. Krien, I. Fiering, Y.-G. Guo, Y. Mei and O. G. Schmidt, *Adv. Mater.*, 2010, **22**, 4591-4595.
48 J. Deng, H. Ji, C. Yan, J. Zhang, W. Si, S. Baunack, S. Oswald, Y. Mei and O. G. Schmidt, *Angew. Chem.*, 2013, **125**, 2382-2386.
49 X. Liu, J. Zhang, W. Si, L. Xi, B. Eichler, C. Yan and O. G. Schmidt, *ACS Nano*, 2015, **9**, 1198-1205.
50 L. Zhang, J. Deng, L. Liu, W. Si, S. Oswald, L. Xi, M. Kundu, G. Ma, T. Gemming, S. Baunack, F. Deng, C. Yan and O. G. Schmidt, *Adv. Mater.*, 2014, **26**, 4527-4532.
51 C. Yan, W. Xi, W. Si, J. Deng and O. G. Schmidt, *Adv. Mater.*, 2013, **25**, 539-544.
52 Y. Chen, C. Yan and O. G. Schmidt, *Adv. Energy Mater.*, 2013, **3**, 1269-1274.
53 X. Sun, C. Yan, Y. Chen, W. Si, J. Deng, S. Oswald, L. Liu and O. G. Schmidt, *Adv. Energy Mater.*, 2014, **4**, 1300912.
54 X. Liu, J. Zhang, W. Si, L. Xi, S. Oswald, C. Yan and O. G. Schmidt, *Nanoscale*, 2015, **7**, 282-288.
55 J. Deng, C. yan, L. Yang, S. Baunack, S. Oswald, H. Wendrock, Y. Mei and O. G. Schmidt, *ACS Nano*, 2013, **7**, 6948-6954.
56 X. Lu, J. Deng, W. Si, X. Sun, X. Liu, B. Liu, L. Liu, S. Oswald, S. Baunack, H. J. Grafe, C. Yan and O. G. Schmidt, *Adv. Sci.*, 2015, 1500113.
57 H. Wu, G. Chan, J. W. Choi, I. Ryu, Y. Yao, M. T. Mcdowell, S. W. Lee, A. Jackson, Y. Yang and L. Hu, *Nat. Nanotechnol.*, 2012, **7**, 310-315.
58 S. W. Lee, H.-W. Lee, I. Ryu, W. D. Nix, H. Gao and Y. Cui, *Nature Comm.,* 2015, **6**, 7533.
59 N. Liu, H. Wu, M. T. McDowell, Y. Yao, C. Wang and Y. Cui, *Nano Lett.*, 2012, **12**, 3315-3321.
60 C. K. Chan, H. Peng, G. Liu, K. McIlwrath, X. F. Zhang, R. A. Huggins, Y. Cui, *Nat. Nanotech.*, 2008, **3**, 31-35.
61 A. Magasinski; P. Dixon; B. Hertzberg; A. Kvit; J. Ayala; G. Yushin, *Nat. Mater.*, 2010, **9**, 353-358.
62 Y. Yao, M. T. McDowell, I. Ryu, H. Wu, N. Liu, L. Hu, W. D. Nix and Y. Cui. *Nano Lett.*, 2011, **11**, 2949-2954.
63 M. Ge, Y. Lu, P. Ercius, J. Rong, X. Feng, M. Mecklenburg and C. Zhou, *Nano Lett.*, 2014, **14**, 261-268.
64 D. S. Jung, T. H. Hwang, S. B. Park, J. W. Choi, *Nano Lett.*, 2013, **13**, 2092-2097.
65 A. Gohier, B. Laïk, K.-H. Kim, J.-L. Maurice, J.-P. Pereira-Ramos, C. S. Cojocaru, P. T. Van, *Adv. Mater.*, 2012, **24**, 2592-2597.
66 B. Wang, X. L. Li, X. F. Zhang, B. Luo, M. H. Jin, M. H. Liang, S. A. Dayeh, S. T. Picraux, L. J. Zhi, *ACS Nano*, 2013, **7**, 1437-1445.
67 S. Guo, S. Dong, *Chem. Soc. Rev.*, 2011, **40**, 2644-2672.
68 D. Wang, Y.-L. Chang, Q. Wang, J. Cao, D. B. Farmer, R. G. Gordon and H. Dai, *J. Am. Chem. Soc.*, 2004, **126**, 11602-11611.
69 J. Graetz, C. C. Ahn, R. Yazami and B. J. Fultz, *Electrochem. Soc.*, 2004, **151**, A698.
70 G. Cui, L. Gu, L. Zhi, N. Kaskhedikar, P. A. van Aken, K. Müllen, and J. Maier, *Adv. Mater.*, 2008, **20**, 3079-3083.
71 S. Choi, J. Kim, N.-S. Choi , M. G. Kim and Soojin Park, *ACS Nano*, 2015, **9**, 2203-2212.
72 T. Kennedy, E. Mullane, H. Geaney, M. Osiak, C. O'Dwyer and K. M. Ryan, *Nano Lett.*, 2014, **14**, 716-723.
73 C. Zhang, Z. Lin, Z. Yang, D. Xiao, P. Hu, H.a Xu, Y. Duan, S. Pang, L. Gu and G. Cui, *Chem. Mater.*, 2015, **27**, 2189-2194.
74 D. Xue, S. Xin, Y. Yan, K.-C. Jiang, Y.-X. Yin, Y.-G. Guo and L.-J. Wan, *J. Am. Chem.Soc.*, 2012, **134**, 2512−2515.
75 J.-G. Ren, Q.-H. Wu, H. Tang, G. Hong, W. Zhang and S.-T. Lee, *J. Mater. Chem. A*, 2013, **1**, 1821-1826.
76 W. Li, M.i Li, Z. Yang, J. Xu, X. Zhong , J. Wang, L. Zeng, X. Liu, Yu Jiang, X. Wei, L. Gu and Y. Yu, *Small*, 2015, **11**, 2762-2767.
77 Y. Sun, S. Jin, G. Yang, J. Wang and C. Wang, *ACS Nano*, 2015, **9**, 3479-3490.
78 J. Liu, K. Song, C. Zhu, C.-C. Chen, P. A. van Aken, J. Maier and Y. Yu, *ACS Nano*, 2014, **8**, 7051-7059.
79 F. Variola, F. Vetrone, L. Richert, P. Jedrzejowski, J. H. Yi, S. Zalzal, S. Clair, A. Sarkissian, D. F. Perepichka, J. D. Wuest, F. Rosei, A. Nanci, *Small*, 2009, **5**, 996-1006.
80 C. K. Chan, X. F. Zhang, Y. Cui, *Nano Lett.*, 2008, **8**, 307-309.
81 M. H. Park, Y. Cho, K. Kim, J. Kim, M. Liu, J. Cho, *Angew. Chem., Int. Ed.*, 2011, **50**, 9647-9650.
82 S. Jin, N. Li, H. Cui, and C. Wang, *Nano Energy*, 2013, **2**, 1128-1136.
83 D. Lv, M. L. Gordin, R. Yi, T. Xu, J. Song, Y.-B. Jiang, D. Choi and D. Wang, *Adv. Funct. Mater.*, 2014, **24**, 1059-1066.
84 X.-L. Wang, W.-Q. Han, H. Chen, J. Bai, T. A. Tyson, X.-Q. Yu, X.-J. Wang, and X.-Q. Yang, *J. Am. Chem. Soc.*, 2011, **133**, 20692-20695.

85 X. Li, J.; Hou, Z. Liang, Y. Zhu, Y. Wang and Y. Qian, *Chem. Commun.*, 2014, **50**, 13956-13959.
86 Y. Son, M. Park, Y. Son, J.-S. Lee, J.-H. Jang, Y. Kim and J. Cho, *Nano Lett.*, 2014, **14**, 1005-1010.
87 S. H. Choi, K. Y. Jung and Y. C. Kang, *ACS Appl. Mater. Interfaces*, 2015, **7**, 13952-13959.
88 H. Qiu, L. Zeng, T. Lan, X. Ding and M. Wei, *J. Mater. Chem. A*, 2015, **3**, 1619-1623.
89 S. Jin, N. Li, H. Cui and C. Wang, *Nano Energy*, 2013, **2**, 1128-1136.
90 H. Wu, M. Xu, H. Wu, J. Xu, Y. Wang, Z. Peng and G. Zheng, *J. Mater. Chem.*, 2012, **22**, 19821-19825.
91 H. B. Wu, J. S. Chen, H. H. Hng and X. W. Lou, *Nanoscale*, 2012, **4**, 2526-2542.
92 J. Liang, H. Hu, H. Park, C. Xiao, S. Ding, U. Paikc and X. W.n Lou, *Energy Environ. Sci.*, 2015, **8**, 1707-1711.
93 Z. bai, Z. Ju, C. Guo, Y. Qian, B. Tang and S. Xiong, *Nanoscale*, 2014, **6**, 3268-3273
94 Y. Zhu, H. Guo, Y. Wu, C. Cao, S. Tao and Z. Wu, *J. Mater. Chem. A*, 2014, **2**, 7904-7911.
95 W. Yang, G. Cheng, C. Dong, Q. Bai, X. Chen, Z. Peng and Z. Zhang, *J. Mater. Chem. A*, 2014, **2**, 20022-20029.
96 N. Wang, L. Chen, X. Ma, J. Yue, F. Niu, H. Xu, J. Yang and Y. Qian, *J. Mater. Chem. A*, 2014, **2**, 16847-16850.
97 L. Liu, H. Guo, J. Liu, F. Qian, C. Zhang, T. Li, W. Chen, X. Yang and Y. Guo, *Chem. Commun.*, 2014, **50**, 9485-9488.
98 Y. Xia, W. Zhang, Z. Xiao, H. Huang, H. Zeng, X. Chen, F. Chen, Y. Gan and X. Tao, *J. Mater. Chem.*, 2012, **22**, 9209-9215.
99 G. Zhou, D.-W. Wang, L.-C. Yin, N. Li, F. Li, and H.-M. Cheng, *ACS Nano*, 2012, **6**, 3214-3223.
100 X.-L. Wang, W.-Q. Han, H. Chen, J. Bai, T. A. Tyson, X.-Q. Yu, X.-J. Wang and X.-Q. Yang, *J. Am. Chem. Soc.*, 2011, **133**, 20692-20695.
101 X. F. Li, X. B. Meng, J. Liu, D. S. Geng, Y. Zhang, M. N. Banis, Y. L. Li, J. L. Yang, R. Y. Li, X. L. Sun, M. Cai and M. W. Verbrugge, *Adv. Funct. Mater.*, 2012, **22**, 1647-1654.
102 K. M. Abraham and Z. J. Jang, *Electrochem. Soc.*, 1996, **143**, 1-5.
103 P. G. Bruce, S. A. Freunberger, L. J. Hardwick and J. M. Tarascon, *Nat. Mater.*, 2012, **11**, 19-29.
104 F. Y. Cheng and J. Chen, *Chem. Soc. Rev.*, 2012, **41**, 2172-2192.
105 F. Li, T. Zhang and H. Zhou, *Energy Environ. Sci.*, 2013, **6**, 1125-1141.
106 H. Jung, J. Hassoun, J. Park, Y. Sun and B. Scrosati, *Nat. Chem.*, 2012, **4**, 579-585.
107 K. Liao, X. Wang, Y. Sun, D. Tang, M. Han, P. He, X. Jiang, T. Zhang and H. Zhou, *Energy Environ. Sci.*, 2015, **8**, 1992-1997.
108 G. Girishkumar, B. McCloskey, A. C. Luntz, S. Swanson and W. Wilcke, *J. Phys. Chem. Lett.*, 2010, **1**, 2193-2203.
109 J. S. Hummelshøj, A. C. Luntz and J. K. Nørskov, *J. Chem. Phys.*, 2013, **138**, 034703.
110 K. Dokko, M. Mohamedi, M. Umeda and I. Uchida, *J. Electrochem. Soc.*, 2003, **150**, A425.
111 L. Mai, Y. Dong, L. Xu and C. Han, *Nano Lett.*, 2010, **10**, 4273-4278.
112 J. Y. Huang, L. Zhong, C. M. Wang, J. P. Sullivan, W. Xu, L. Q. Zhang, S. X. Mao, N. S. Hudak, X. H. Liu, A. Subramanian, H. Fan, L. Qi, A. Kushima and J. Li, *Science*, 2010, **330**, 1515-1520.
113 J. W. Wang, Y. He, F. Fan, X. H. Liu, S. Xia, Y. Liu, C. T. Harris, H. Li, J. Y. Huang, S. X. Mao and T. Zhu, *Nano Lett.*, 2013, **13**, 709-715.
114 M. T. McDowell and Y. Cui, *Adv. Energy Mater.*, 2011, **1**, 894-900.
115 W. Si, I. Mönch, C. Yan, J. Deng, S. Li, G. Lin. L. Han, Y. Mei and O. G. Schmidt, *Adv. Mater.*, 2014, **26**, 7973-7978.
116 X. Xu, M. Yan, X. Tian, C. Yang, M. Shi, Q. Wei, L. Wu and L. Mai, *Nano Lett.*, 2015, **15**, 3879-3884.
117 X.Lu, J. Deng, W, Si, X. Sun, X. Liu, B. Liu, L. Liu, S. Oswald, S. Baunack, H. J. Grafe, C. Yan and O. G. Schmidt, *Adv. Sci.*, 2015, **2**, 1500113.
118 M. Belleville, E. Cantatore, H. Fanet, P. Fiorini, P. Nicole, M. Pelgrom, C. Piguet, R. Hahn, C. V. Hoof and R. Vullers, *Rep. CATRENE Work. Group Energy Auton. Syst.* 2009.
119 R. Sharma, C. C. B. Bufon, D. Grimm, R. Sommer, A. Wollatz, J. Schadewald, D. J. Thurmer, P. F. Siles, M. Bauer and O. G. Schmidt, *Adv. Energy Mater.*, 2014, **4**, 1301631.
120 E. J. Smith, W. Xi, D. Makarov, I. Mönch, S. Harazim, V. A. B. Quiñones, C. K. Schmidt, Y. Mei, S. Sanchez and O. G. Schmidt, *Lab Chip*, 2012, **12**, 1917-1931.
121 B. Nikoobakht and X. L. Li, *ACS Nano*, 2012, **6**, 1883-1887.
122 C. C. B. Bufon, J. D. C. González, D. J. Thurmer, D. Grimm, M. Bauer and O. G. Schmidt, *Nano Lett.*, 2010, **10**, 2506-2510.
123 V. Augustyn, J. Come, M. A. Lowe, J. W. Kim, P.-L. Taberna, S. H. Tolbert, H. D. Abruña, P. Simon and B. Dunn, *Nat. Mater.*, 2013, **12**, 518-522.
124 L. Wang, B. Liu, S. Ran, H. Huang, X. Wang, B. Liang, D. Chen and G. Shen, *J. Mater. Chem.*, 2012, **22**, 23541-23546,
125 Y. Fu, Q. Wei, X. Wang, H. Shu, X. Yang and S. Sun, *J. Mater. Chem. A*, 2015, **3**, 13807-13818.
126 J. Liang, H. Hu, H. Park, C. Xiao, S. Ding, U. Paik and X. W. (David) Lou, *Energy Environ. Sci.*, 2015, **8**, 1707-1711.
127 X. Liu, W. Si, J. Zhang, X. Sun, J. Deng, S. Baunack, S. Oswald, L. Liu, C. Yan and O. G. Schmidt, *Sci. Rep.*, 2014, **4**, 7452.
128 A. L. M. Reddy, S. R. Gowda, M. M. Shaijumon and P. M. Ajayan, *Adv. Mater.*, 2012, **24**, 5045-5064.
129 L. Su, Y. Zhong and Z. Zhou, *J. Mater. Chem. A*, 2013, **1**, 15158-15166.
130 B. Qu, L. Hu, Y. Chen, C. Li, Q. Li, Y. Wang, W. Wei, L. Chen and T. Wang, *J. Mater. Chem. A*, 2013, **1**, 7023-7026.
131 X. Sun, W. Si, X. Liu, J. Deng, L. Xi, L. Liu, C. Yan and O. G. Schmidt, *Nano Energy*, 2014, **9**, 168-175.
132 Y. Yu, C. Yan, L. Gu, X. Lang, K. Tang, L. Zhang, Y. Hou, Z. Wang, M. W. Chen, O. G. Schmidt and J. Maier, *Adv. Energy Mater.*, 2013, **3**, 281-285.
133 X. Yang, C. Cheng, Y. Wang, L. Qiu and D. Li, *Science*, 2013, **341**, 534-537.
134 H. Wang, L.-F. Cui, Y. Yang, H. Sanchez Casalongue, J. T. Robinson, Y. Liang, Y. Cui and H. Dai, *J. Am. Chem. Soc.*, 2010, **132**, 13978-13980.
135 P. Xiong, B. Liu, V. Teran, Y. Zhao, L. Peng, X. Wang and G. Yu, *ACS Nano*, 2014, **8**, 8610-8616.
136 P. XIong, L. Peng, D. Chen, Y. Zhao, X. Wang and G. Yu, *Nano Energy*, 2015, **12**, 816-823.
137 A. Yu, I. Roes, A. Davies and Z. Chen, *Appl. Phys. Lett.*, 2010, **96**, 253105.
138 T. Chen, Y. Xue, A. K. Roy and L. Dai, *ACS Nano*, 2014, **8**, 1039-1046.
139 P. Xu, J. Kang, J.-B. Choi, J. Suhr, J. Yu, F. Li, J.-H. Byun, B.-S. Kim and T. W. Chou, *ACS Nano*, 2014, **8**, 9437-9445.
140 N. Li, G. Yang, Y. Sun, H. Song, H. Cui, G. Yang and C. Wang, *Nano Lett.*, 2015, **15**, 3195-3203.
141 H. Y. Jung, M. B. Karimi, M. G. Hahm, P. M. Ajayan and Y. J. Jung, *Sci. Rep.*, 2012, 2.
142 J. J. Yoo, K. Balakrishnan, J. Huang, V. Meunier, B. G. Sumpter, A. Srivastava, M. Conway, A. L. M. Reddy, J. Yu, R. Vajtai and P. M. Ajayan, *Nano Lett.*, 2011, **11**, 1423-1427.
143 Y. He, W. Chen, X. Li, Z. Zhang, J. Fu, C. Zhao and E. Xie , *ACS Nano*, 2013, **7**, 174-182.
144 P. C. Chen, H. T. Chen, J. Qiu and C. W. Zhou, *Nano Res.*, 2010, **3**, 594-603.
145 X. Wang, X. Lu, B. Liu, X. Tong and G. Shen, *Adv. Mater.*, 2014, **26**, 4763-4782.

146 Y. Shi, L. Peng, Y. Ding, Y. Zhao and G. Yu, *Chem. Soc. Rev*., 2015, **44**, 6684-6696.
147 J. A. Lee, M. K. Shin, S. H. Kim, S. J. Kim, G. M. Spinks, G. G. Wallace, R. Ovalle-Robles, M. D. Lima, M. E. Kozlov and R. H. Baughman, *ACS Nano*, 2012, **6**, 327-334.
148 M. Kaempgen, C. K. Chan, J. Ma, Y. Cui and G. Gruner, *Nano Lett.*, 2009, **9**, 1872-1876.
149 Y. F. Xu, M. G. Schwab, A. J. Strudwick, J. Hennig, X. L. Feng, Z. S. Wu and K. Müllen, *Adv. Energy Mater.*, 2013, **3**, 1035-1040.
150 Z.-S. Wu, Z. Liu, K. Parvez, X. Feng and L. Müllen, *Adv. Mater.*, 2015, **27**, 3669-3675.
151 X. Lang, A. Hirata, T. Fujita and M. Chen, *Nat. Nanotech*., 2011, **6**, 232-236.
152 P. Simon and Y. Gogotsi, *Nature Mater.*, 2008, **7**, 845-854.
153 M. Beidaghi and Y. Gogotsi, *Energy Environ. Sci.*, 2014, **7**, 867-884.
154 J. Chmiola, C. Largeot, P.-L. Taberna, P. Simon and Y. Gogosti, *Science*, 2010, **328**, 480-483.
155 D. Pech, M. Brunet, H. Durou, P. Huang, V. Mochalin, Y. Gogotsi, P.-L. Taberna and P. Simon, *Nat Nanotechnol.*, 2010; **5**, 651-655.
156 K. Wang, W. Zou, B. Quan, A. Yu, H. Wu, P. Jiang and Z. Wei, *Adv. Energy Mater.*, 2011, **1**, 1068-1072.
157 L. Cao, S. Yang, W. Gao, Z. Liu, Y. Gonf, L. Ma, G. Shi, S. Lei, Y. Zhang, S. Zhang, R. Vajtai and P. M. Ajayan, *Small*, 2013, **9**, 2905-2910.
158 W. Gao, N. Singh, L. Song, Z. Liu, A. L. M. Reddy, L. Ci, R. Vajtai, Q. Zhang, B. Wei and P. M. Ajayan, *Nat Nanotechnol.*, 2011, **6**, 496-500.
159 M. F. El-Kady and R. B. Kaner, *Nat Commun.*, 2013, **4**, 1475.
160 Y. Gogotsi and P. Simon, *Science*, 2011, **334**, 917- 918.
161 Z. Niu, L. Zhang, L. Liu, B. Zhu, H. Dong and X. Chen, *Adv. Mater.*, 2013, **25**, 4035-4042.
162 Z.-S. Wu, K. Parvez, X. Feng and K. Müllen, *Nat. Comm.*, 2013, **4**, 2487.
163 Z. P. Zhang, J. Zhang, N. Chen, L. T. Qu, *Energy Environ. Sci.*, 2012, **5**, 8869-8890.
164 W. Liu, Y.-Q. Feng, X.-B. Yan, J.-T. Chen and Q.-J. Xue, *Adv. Funct. Mater.*, 2013, **23**, 4111-4122.
165 S. Chen, J. W. Zhu, X. D. Wu, Q. F. Han, X. Wang, *ACS Nano*, 2010, **4**, 2822-2830.
166 X. Wang, B. D. Myers, J. Yan, G. Shekhawat, V. Dravid and P. S. Lee, *Nanoscale*, 2013, **5**, 4119-4122.
167 W. Si, C. Yan, Y. Chen, S. Oswald, L. Han and O. G. Schmidt, *Energy Environ. Sci.*, 2013, **6**, 3218-3223.
168 L. Peng, X. Peng, B. Liu, C. Wu, Y. Xie and G. Yu, *Nano Lett.*, 2013, **13**, 2151-2157.